Heat bath particle number spectrum

P. Jizba*
DAMTP, University of Cambridge, Silver Street, Cambridge, CB3 9EW, United Kingdom
(Received 16 June 1997; published 11 February 1998)

We calculate the number spectrum of particles radiated during a scattering into a heat bath using the thermal largest-time equation and the Dyson-Schwinger equation. We show how one can systematically calculate $d\langle N(\omega)\rangle/d\omega$ to any order using modified real-time finite-temperature diagrams. Our approach is demonstrated on a simple model where two scalar particles scatter, within a photon heat bath, into a pair of charged particles and it is shown how to calculate the resulting changes in the number spectra of the photons. [S0556-2821(98)05304-1]

PACS number(s): 11.10.Wx, 12.38.Mh

I. INTRODUCTION

In recent years much theoretical effort has been invested in the understanding of relativistic heavy ion collisions as these can create critical energy densities which are large enough to produce the quark-gluon plasma (the deconfined phase of quarks and gluons) [1,2]. A natural tool for testing the quark-gluon plasma properties would be to look for the particle number spectrum formed when a particle decays within the plasma itself. As the plasma created during heavy ion collisions is, to a very good approximation, in thermodynamical equilibrium [1] (somewhat like a ''microwave oven'' or a heat bath), one can use the whole machinery of statistical physics and quantum field theory (QFT) in order to predict the final plasma number spectrum. Such calculations, derived from first principles, were carried out by Landshoff and Taylor [3].

Our aim was to find a sufficiently easy mathematical formalism allowing us to perform the mentioned calculations to any order. Because unstable particles treated in [3] cannot naturally appear in asymptotic states, we demonstrate our approach on a mathematically more correct (but from a practical point of view less relevant) process: namely, on the scattering of two particles inside of a heat bath. The method presented here, however, might be applied as well to a decay itself (provided that the corresponding decay rate is much less than any of the characteristic energies of the process). In this paper we formulate the basic diagrammatic rules for the methodical perturbative calculus of the plasma particle number spectrum $d\langle N(\omega)\rangle/d\omega$ and discuss it in the simple case of a heat bath comprised of photons and electrons, which are for simplicity treated as scalar particles.

In Sec. II we review the basic concepts and techniques needed from the theory of the largest-time equation (both for $T=0$ and $T\neq 0$) and the Dyson-Schwinger equation. Rules for the cut diagrams at finite temperature are derived and subsequently extended to the case when unheated fields are present. It was already pointed out in [4] that the thermal cut diagrams are virtually the Kobes-Semenoff diagrams [1] in the Keldysh formalism [5]. This observation will allow us to identify type-1 vertices in the real-time finite-temperature diagrams with the uncircled vertices used in the (thermal) cut diagrams, and similarly type-2 vertices will be identified with the circled, cut diagram vertices. As we want to restrict our attention to only some particular final particle states, further restrictions on the possible cut diagrams must be included. We shall study these restrictions in the last part of Sec. II.

As we shall show in Sec. III, the heat bath particle number spectrum can be conveniently expressed as a fraction. While it is possible to compute the denominator by means of the thermal cut diagrams developed in Sec. II, the calculation of the numerator requires more care. Using the Dyson-Schwinger equation, we shall see in Sec. IV that it can be calculated through modified thermal cut diagrams. The modification consists of the substitution in turn of each heat bath particle propagator by an altered one. We also show that there must be only one modification per diagram. From this we conclude that from each individual cut diagram we get n modified ones (n stands for the total number of heat bath particle propagators in the diagram). Furthermore, in the case when more types of heat bath particles are present, one might be only interested in the number spectrum of some of these. The construction of the modified cut diagrams in such cases follows the same procedure as in the previous situation. We find that only the propagators affiliated to the desired fields must be altered.

In Sec. V the presented approach is applied to a toy model in which a gluon plasma is simulated by scalar photons, and we calculate the resulting changes in the number spectrum of the ''plasma'' particles. Section V ends with a qualitative discussion of the quark-gluon plasma simulated by scalar photons and electrons.

Finally, in the Appendix we derive, directly from the thermal Wick's theorem, the (thermal) Dyson-Schwinger equation as well as other useful functional identities valid at finite temperature.

II. BASIC TOOLS

A. Mean statistical value

The central idea of thermal QFT is based on the fact that one cannot take the expectation value of an observable A with respect to some pure state as generally all states have nonzero probability to be populated and consequently one

*Email address: pj10006@damtp.cam.ac.uk

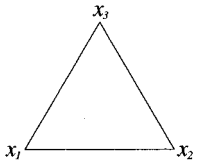

FIG. 1. A one-loop triangle diagram.

must consider instead a mixture of states generally described by the density matrix ρ. The mean statistical value of A is then

$$\langle A\rangle = \mathrm{Tr}(\rho A), \tag{2.1}$$

where the trace has to be taken over a complete set of *physical* states. For a statistical system in thermodynamical equilibrium ρ is given by the Gibbs canonical distribution

$$\rho = \frac{e^{-\beta(H-\mu N)}}{\mathrm{Tr}(e^{-\beta(H-\mu N)})} = \frac{e^{-\beta K}}{Z}; \tag{2.2}$$

here, Z is the partition function, H is the Hamiltonian, N is the conserved charge (e.g., baryon or lepton number), μ is the chemical potential, $K=H-\mu N$, and β is the inverse temperature: $\beta=1/T$ $(k_B=1)$.

B. Largest-time equation at $T=0$

An important property inherited from zero-temperature QFT is *the largest-time equation* (LTE) [6–8]. Although the following sections will mainly hinge on the *thermal* LTE, it is instructive to start first with the zero-temperature one. The LTE at $T=0$ is a generally valid identity which holds for any individual diagram constructed with propagators satisfying certain simple properties. For instance, for the scalar theory with a coupling constant g one can define the following rules:

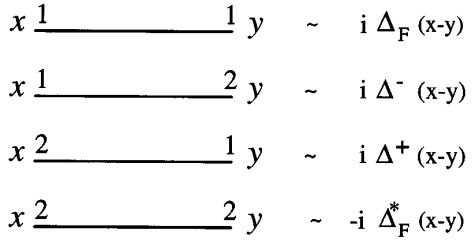

Here $i\Delta_F$ is the Feynman propagator, $i\Delta^+$ $(i\Delta^-)$ is corresponding positive (negative) energy part of $i\Delta_F$, the asterisk means complex conjugation, and index 1 (2) denotes a *type-1* (*type-2*) vertex; the type-1 vertex has attached a factor $-ig$ while the type-2 vertex bears a factor ig. Using this prescription, we can construct diagrams in configuration space. With each diagram then can be associated a function $F(x_1,\ldots x_n)$ having all the second type vertices underlined. For example, for the triangle diagram in Fig. 1 we have

$$F(x_1,x_2,x_3) = (-ig)^3 i\Delta_F(x_1-x_2)i\Delta_F \times (x_1-x_3)i\Delta_F(x_2-x_3),$$

$$F(\underline{x_1},x_2,x_3) = (-ig)^2(ig)i\Delta^+(x_1-x_2)i\Delta^+ \times (x_1-x_3)i\Delta_F(x_2-x_3),$$

$$F(\underline{x_1},\underline{x_2},x_3) = (ig)^2(-ig)(-i)\Delta_F^*(x_1-x_2)i\Delta^+ \times (x_1-x_3)i\Delta^+(x_2-x_3),$$

$$F(\underline{x_1},\underline{x_2},\underline{x_3}) = (ig)^3(-i)\Delta_F^*(x_1-x_2)(-i)\Delta_F^* \times (x_1-x_3)(-i)\Delta_F^*(x_2-x_3),$$

etc.

The LTE then states that for a function $F(x_1,\ldots,x_n)$ corresponding to some diagram with n vertices

$$F(\ldots,\underline{x_i},\ldots)+F(\ldots,x_i,\ldots)=0, \tag{2.3}$$

provided that x_{i0} is the largest time and all other underlinings in F are the same. The proof of Eq. (2.3) is based on an observation that the propagator $i\Delta_F(x)$ can be decomposed into positive and negative energy parts, i.e.,

$$i\Delta_F(x)=\theta(x_0)i\Delta^+(x)+\theta(-x_0)i\Delta^-(x), \tag{2.4}$$

$$i\Delta^{\pm}(x)=\int \frac{d^4k}{(2\pi)^3}e^{-ikx}\theta(\pm k_0)\,\delta(k^2-m^2). \tag{2.5}$$

Incidentally, for x_{i0} being the largest time this directly implies

$$i\Delta_F(x_j-x_i)=i\Delta^-(x_j-x_i),$$

$$-i\Delta_F^*(x_i-x_j)=i\Delta^-(x_i-x_j),$$

$$i\Delta_F(0)=-i\Delta_F^*(0). \tag{2.6}$$

As $F(\ldots,\underline{x_i},\ldots)$ differs from $F(\ldots,x_i,\ldots)$ only in the propagators directly connected to x_i—which are equal [see Eq. (2.6)]—and in the sign of the x_i vertex, they must mutually cancel.

Summing up Eq. (2.3) for all possible underlinings (excluding x_i), we get the LTE where the special role of the largest time is not manifest any more, namely,

$$\sum_{\text{index}} F(x_1,x_2,\ldots,x_n)=0. \tag{2.7}$$

The sum Σ_{index} means summing over all possible distributions of indices 1 and 2 (or equivalently over all possible underlinings). The zero-temperature LTE can be easily reformulated for the T matrices. Let us recall that the Feynman diagrams for the S matrix $(S=1+iT)$ can be obtained by multiplying the corresponding $F(x_1,\ldots,x_n)$ with the plane waves for the incoming and outgoing particles, and subsequently integrate over $x_1,\ldots,x_n$. Thus, in fixed volume quantization a typical n-vertex Feynman diagram is given by

$$\int \prod_{i=1}^{n} dx_i \prod_j \frac{e^{-ip_j x_{m_j}}}{\sqrt{2\omega_{p_j} V}} \prod_k \frac{e^{iq_k x_{m_k}}}{\sqrt{2\omega_{q_k} V}} F(x_1,\ldots,x_n). \tag{2.8}$$

Here the momenta $\{p_j\}$ are attached to incoming particles at the vertices $\{x_{m_j}\}$, while momenta $\{q_k\}$ are attached to outgoing particles at the vertices $\{x_{m_k}\}$. In order to distinguish among various functions $F(x_1,\ldots,x_n)$ with the same variables $x_1,\ldots,x_n$, we shall attach a subscript l_n to each function F. For instance, the function $F_{1_4}(x_1,\ldots,x_4)$ corresponding to the diagram

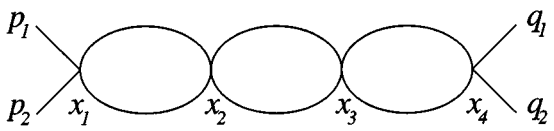

contributes to $\langle q_1 q_2|iT|p_1 p_2\rangle$ by

$$\int \prod_{i=1}^{4} dx_i \frac{e^{-i(p_1+p_2)x_1}}{V\sqrt{4\omega_{p_1}\omega_{p_2}}} \frac{e^{i(q_1+q_2)x_4}}{V\sqrt{4\omega_{q_1}\omega_{q_2}}} \times [i\Delta_F(x_1-x_2)]^2 [i\Delta_F(x_2-x_3)]^2 [i\Delta_F(x_3-x_4)]^2;$$

similarly, the function $F_{2_4}(x_1,\ldots,x_4)$ corresponding to the diagram

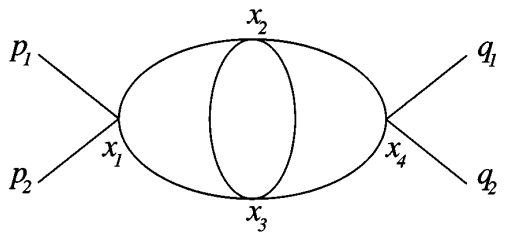

contributes to $\langle q_1 q_2|iT|p_1 p_2\rangle$ by

$$\int \prod_{i=1}^{4} dx_i \frac{e^{-i(p_1+p_2)x_1}}{V\sqrt{4\omega_{p_1}\omega_{p_2}}} \frac{e^{i(q_1+q_2)x_4}}{V\sqrt{4\omega_{q_1}\omega_{q_2}}} i\Delta_F(x_1-x_2) i\Delta_F \times (x_1-x_3)[i\Delta_F(x_2-x_3)]^2 \times i\Delta_F(x_4-x_3) i\Delta_F(x_4-x_2),$$

etc.

This can be summarized as

$$\langle\{q_k\}|iT|\{p_j\}\rangle = \sum_n \int \cdots \int \prod_{i=1}^{n} dx_i \sum_{l_n} \prod_j \frac{e^{-ip_j x_{m_j}}}{\sqrt{2\omega_{p_j} V}} \times \prod_k \frac{e^{iq_k x_{m_k}}}{\sqrt{2\omega_{q_k} V}} F_{l_n}(x_1,\ldots,x_n). \tag{2.9}$$

Consider now the case $|\{p_j\}\rangle = |\{q_k\}\rangle$ (let us call it $|a\rangle$). From the unitarity condition $T - T^\dagger = iT^\dagger T$, we get

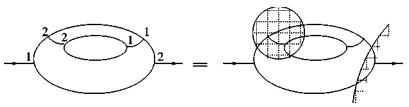

FIG. 2. An example of a cut diagram in the φ^3 theory which does not contribute to the RHS's of Eqs. (2.12) and (2.13). Arrows indicate the flow of energy.

$$\langle a|T|a\rangle - \langle a|T|a\rangle^* = i\langle a|T^\dagger T|a\rangle. \tag{2.10}$$

On the other hand, by construction $F(\underline{x_1},\ldots,\underline{x_n}) = F^*(x_1,\ldots,x_n)$, and thus [see Eq. (2.7)]

$$F(x_1,\ldots,x_n) + F^*(x_1,\ldots,x_n) = -\sum_{\text{index}'} F(x_1,\ldots,x_n). \tag{2.11}$$

The prime over ''index'' in Eq. (2.11) indicates that we sum neither over diagrams with all type-1 vertices nor diagrams with all type-2 vertices. Using Eq. (2.9) and identifying $|\{q_k\}\rangle$ with $|\{p_k\}\rangle$ $(=|a\rangle)$ we get

$$\langle a|T|a\rangle - \langle a|T|a\rangle^* = -\sum_{\text{index}'} \langle a|T|a\rangle \tag{2.12}$$

or [see Eq. (2.10)]

$$\langle a|T^\dagger T|a\rangle = i\sum_{\text{index}'} \langle a|T|a\rangle. \tag{2.13}$$

Equation (2.12) is the special case of the LTE for the T matrices. The finite-temperature extension of Eq. (2.13) will prove crucial in Sec. IV.

Owing to the $\theta(\pm k_0)$ in $\Delta^{\pm}(x)$ [see Eq. (2.5)], energy is forced to flow only towards type-2 vertices. From both the energy-momentum conservation in each vertex and from the energy flow on the external lines, a sizable class of the diagrams on the right hand sides (RHS's) of Eqs. (2.12) and (2.13) will be automatically zero. Particularly regions of either first or second type vertices which are not connected to any external line violate the energy conservation and thus do not contribute (no islands of vertices); see Fig. 2. Consequently, the only surviving diagrams are those whose any first type vertex area is connected to incoming particles and any second type vertex area is connected to outgoing ones. From historical reasons the border between two regions with different type of vertices is called a *cut* and corresponding diagrams are called *cut diagrams*.

We have just proved a typical feature of $T=0$ QFT; namely, any cut diagram is divided by the cut into two areas only; see Fig. 3. Equation (2.12), rewritten in terms of the cuttings, is the so-called *cutting equation* (or Cutkosky's cut-

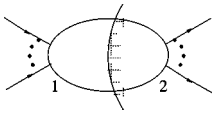

FIG. 3. Generic form of the cut diagram at the $T=0$. The shadow is on the second type vertex area.

ting rules) [6–8]. One point should be added. Inserting the completeness relation $\Sigma_f|f\rangle\langle f|=1$ into the LHS of Eq. (2.13), we get

$$\sum_f \langle a|T^\dagger|f\rangle\langle f|T|a\rangle = i\sum_{\text{cuts}} \langle a|T|a\rangle. \tag{2.14}$$

It may be shown [4,6] that all the intermediate particles in $|f\rangle$ correspond to cut lines. This has a natural extension when $\langle a|T^\dagger T|a\rangle \to \langle a|T^\dagger \mathcal{P} T|a\rangle$ with $\mathcal{P}$ being a projection operator ($\mathcal{P}=\mathcal{P}^\dagger=\mathcal{P}^2$) which eliminates some of the states $|f\rangle$. It is easy to see that in such a case

$$\langle a|T^\dagger \mathcal{P} T|a\rangle = i\tilde{\sum_{\text{cuts}}} \langle a|T|a\rangle, \tag{2.15}$$

where tilde over Σ_{cuts} indicates that one sums over the diagrams which do not have cut lines corresponding to particles removed by $\mathcal{P}$.

There is no difficulty in applying the previous results to spin-$\frac{1}{2}$ [6,7]. The LTE follows as before: The diagram with only iS_F propagators (and $-ig$ per each vertex) plus the diagram with only ($i\hat{S}_F$) propagator[1] (and ig per each vertex) equals minus the sum of all diagrams with one up to $n-1$ type-2 vertices (n being the total number of vertices). For gauge fields more care is needed. Using the Ward identities one can show [6] that type-1 and type-2 vertices in Eqs. (2.12) and (2.13) may be mutually connected only by *physical particle* propagators [i.e., neither through the propagators corresponding to particles with nonphysical polarizations nor Faddeev-Popov (FP) ghosts and antighosts].

C. Thermal Wick's theorem (the Dyson-Schwinger equation)

The key observation at finite temperature is that for systems of *noninteracting* particles in thermodynamical equilibrium Wick's theorem is still valid; i.e., one can decompose the $2n$-point (free) thermal Green function into a product of two-point (free) thermal Green functions. This may be defined recursively by

$$\langle \mathcal{T}[\psi(x_1)\cdots\psi(x_{2n})]\rangle_\beta = \sum_{j\neq i} \varepsilon_P \langle \mathcal{T}[\psi(x_i)\psi(x_j)]\rangle_\beta \times \left\langle \mathcal{T}\left(\prod_{k\neq i;j} \psi(x_k)\right)\right\rangle_\beta, \tag{2.16}$$

where ε_P is the signature of the permutation of fermion operators ($=1$ for boson operators) and $\mathcal{T}$ is the standard time ordering symbol. We shall use, from now on, the subscript β, emphasizing that the thermal mean value describes a system in thermodynamical equilibrium (at the temperature β^{-1}). Note that the choice of ''i'' in Eq. (2.16) is completely arbitrary. The proof can be found, for example, in [1,9,10].

[1]The function $i\hat{S}_F(x)$, similarly as $(i\Delta_F)^*(x)$, interchanges the roles of S^+ and S^-. Unlike bosons, for fermions $i\hat{S}_F(x)$ is not equal to $(iS_F)^*(x)$. Despite that, Eq. (2.12) still holds [6].

Similarly as at $T=0$, Wick's theorem can also be written for the (free) thermal Wightman functions [9,11], i.e.,

$$\langle \psi(x_1)\cdots\psi(x_{2n})\rangle_\beta = \sum_{j\neq 1} \varepsilon_P \langle \psi(x_1)\psi(x_j)\rangle_\beta \times \left\langle \prod_{k\neq 1;j} \psi(x_k)\right\rangle_\beta. \tag{2.17}$$

A particularly advantageous form of this is the so-called Dyson-Schwinger equation (see the Appendix) which, at $T\neq 0$, reads

$$\langle G[\psi]\psi(x)F[\psi]\rangle_\beta = \int dz \langle \psi(x)\psi(z)\rangle_\beta \left\langle G[\psi]\frac{\vec{\delta}F[\psi]}{\delta\psi(z)}\right\rangle_\beta + \int dz \langle \psi(z)\psi(x)\rangle_\beta \times \left\langle \frac{G[\psi]\overleftarrow{\delta}}{\delta\psi(z)}F[\psi]\right\rangle_\beta, \tag{2.18}$$

where $\psi(x)$ is an interaction-picture field and $G[\cdots]$ and $F[\cdots]$ are functionals of ψ. The arrowed variations $\delta/\delta\psi(z)$ are defined as a formal operation satisfying two conditions: namely,

$$\frac{\vec{\delta}}{\delta\psi_n(z)}[\psi_m(x)\psi_q(y)] = \frac{\delta\psi_m(x)}{\delta\psi_n(z)}\psi_q(y) + (-1)^p\psi_m(x)\frac{\delta\psi_q(y)}{\delta\psi_n(z)} \tag{2.19}$$

or

$$[\psi_m(x)\psi_q(y)]\frac{\overleftarrow{\delta}}{\delta\psi_n(z)} = (-1)^p\frac{\delta\psi_m(x)}{\delta\psi_n(z)}\psi_q(y) + \psi_m(x)\frac{\delta\psi_q(y)}{\delta\psi_n(z)}, \tag{2.20}$$

with

$$\frac{\delta\psi_m(x)}{\delta\psi_n(y)} = \delta(x-y)\,\delta_{mn}. \tag{2.21}$$

The p is 0 for bosons and 1 for fermions; subscripts m,n suggest that several types of fields can be generally present. Note, for bosons, $\vec{\delta}F/\delta\psi = F\overleftarrow{\delta}/\delta\psi$ which we shall denote as $\delta F/\delta\psi$. For more details see the Appendix.

D. Thermal largest-time equation

The LTE (2.13) can be extended to the finite-temperature case, too. Summing up in Eq. (2.13) over all the eigenstates of $K(=H-\mu N)$ with the weight factor $e^{-\beta K_i}$ (i labels the eigenstates), we get

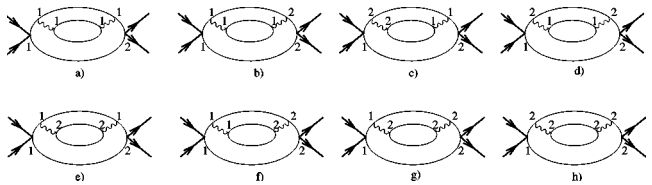

FIG. 4. An example of nonvanishing cut diagrams at the $T \neq 0$. The heat bath consists of two different particles. External particles are not thermalized.

$$\langle TT^{\dagger}\rangle_{\beta} = i \sum_{\text{index}'} \langle T\rangle_{\beta}. \tag{2.22}$$

Let us consider the RHS of Eq. (2.22) first. The corresponding thermal LTE and diagrammatic rules (Kobes-Semenoff rules [1]) can be derived precisely the same way as at $T=0$ using the previous, largest-time argumentation [1,12]. It turns out that these rules have basically an identical form as those in the previous section, with an exception that now $\langle 0|\cdots|0\rangle \to \langle \cdots \rangle_{\beta}$. Note that labeling vertices by 1 and 2 we have naturally got a doubling of the number of degrees of freedom. This is a typical feature of the *real-time formalism* in thermal QFT (here, in the so-called *Keldysh version* [1]).

We should also emphasize that it may happen that some fields are not thermalized. For example, external particles entering a heat bath or particles describing nonphysical degrees of freedom [13]. Particularly, if some particles (with momenta $\{p_j\}$) enter the heat bath, the mean statistical value of an observable A is then

$$\sum_i \frac{e^{-\beta K_i}}{Z} \langle i;\{p_j\}|A|i;\{p_j\}\rangle = Z^{-1}\mathrm{Tr}(\rho_{\{p_j\}} \otimes e^{-\beta K} A),$$

$$\rho_{\{p_j\}} = |\{p_j\}\rangle\langle\{p_j\}|,$$

which we shall denote as $\langle A\rangle_{\{p_j\},\beta}$. From this easily follows the generalization of Eq. (2.22),

$$\langle TT^{\dagger}\rangle_{\{p_k\},\beta} = i \sum_{\text{index}'} \langle T\rangle_{\{p_k\},\beta}. \tag{2.23}$$

Unlike $T=0$, we find that the cut diagrams have disconnected vertex areas and no kinematic reasonings used in last section can, in general, get rid of them. This is because the thermal part[2] of $\langle \varphi(x)\varphi(y)\rangle_{\beta}$ describes the absorption of on-shell particle from the heat bath or the emission of one into it. Thus, at $T \neq 0$, there is no definite direction of transfer of energy from a type-1 vertex to a type-2 one as energy flows in both directions. Some cut diagrams nevertheless vanish. It is simple to see that only those diagrams survive in which the nonthermalized external particles ''enter'' a diagram via the first type vertices and ''leave'' it via the second type ones. We might deduce this from the definition of $\langle T\rangle_{\{p_j\},\beta}$; indeed,

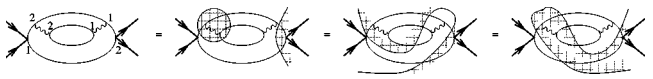

FIG. 5. The cut diagram from Fig. 3(c) demonstrates that the cut can be defined in many ways but the number of crossed lines is still the same.

$$\sum_{\text{index}'} \langle T\rangle_{\{p_j\},\beta} = \sum_{\text{index}'} \sum_i \frac{e^{-\beta K_i}}{Z} \langle i;\{p_j\}|T|i;\{p_j\}\rangle. \tag{2.24}$$

Note that we get the same set of thermal cut diagrams interchanging the summation $\Sigma_{\text{index}'}$ with Σ_i. It is useful to start then with $\Sigma_{\text{index}'}\langle i;\{p_j\}|T|i;\{p_j\}\rangle$. This is, as usual, described by the $(T=0)$ cutting rules. In the last section we learned that the general structure of the corresponding cut diagrams is depicted in Fig. 3; particularly the external particles enter the cut diagram via type-1 vertices and leave it via type-2 ones. Multiplying each diagram (with the external particles in the state $|i;\{p_j\}\rangle$) with the prefactor $e^{-\beta K_i}/Z$ and summing subsequently over i, we again retrieve the thermal cut diagrams, though now it becomes evident that the particles $\{p_j\}$ enter such a diagram only via type-1 vertices and move off only through type-2 ones, since the summation of the $(T=0)$ cut diagrams from which it was derived does not touch lines corresponding to unheated particles. Note that the latter analysis naturally explains why the unheated particles obey the $(T=0)$ LTE diagrammatic rules even in the thermal diagrams

Another vanishing comes from kinematic reasons. Namely, three-leg vertices with all on-shell particles (1–2 lines) cannot conserve energy and momentum and consequently the whole cut diagram is zero. As an illustration let us consider all the nonvanishing, topologically equivalent cut diagrams[3] of given type involved in a three-loop contribution to $i\Sigma_{\text{index}'}\langle T\rangle_{pq,\beta}$ (see Fig. 4).

Let us stress one more point. In contrast with $T=0$, at finite temperature the cut itself neither is unique nor defines topologically equivalent areas (see Fig. 5); only the number of crossed legs is, by definition, invariant. This ambiguity shows that the concept of the cut is not very useful at finite temperature and in the following we shall refrain from using it.

In Sec. IV it will prove useful to have an analogy of Eq. (2.23) for $\langle T^{\dagger}\mathcal{P}T\rangle_{\beta}$. Here $\mathcal{P}$ is the projection operator defined as

$$\mathcal{P} = \sum_j |a;j\rangle\langle a;j|, \tag{2.25}$$

where j denotes the physical states for the heat bath particles and a labels the physical states for the outgoing, nonthermalized particles. Let us deal with $\langle T^{\dagger}\mathcal{P}T\rangle_{\beta}$. Using Eq. (2.15), we acquire

[2]Note that $\langle \varphi(x)\varphi(y)\rangle_{\beta} = \langle :\varphi(x)\varphi(y):\rangle_{\beta} + \langle 0|\varphi(x)\varphi(y)|0\rangle$ and $\langle :\varphi(x)\varphi(y):\rangle_{\beta} = \int [d^4k/(2\pi)^3] f_B(k_0)\delta(k^2-m^2)e^{-ik(x-y)}$, with $f_B(k_0) = (e^{\beta|k_0|}-1)^{-1}$.

[3]Let us emphasize that originally we had 64 possible cut diagrams.

$$\langle T^\dagger \mathcal{P} T\rangle_\beta = i\sum_l \frac{e^{-\beta K_l}}{Z} \tilde{\sum_{\text{index}'}} \langle l|T|l\rangle. \tag{2.26}$$

Interchanging the summations, we finally arrive at

$$\langle T^\dagger \mathcal{P} T\rangle_\beta = i \tilde{\sum_{\text{index}'}} \langle T\rangle_\beta, \tag{2.27}$$

where tilde over the $\Sigma_{\text{index}'}$ means that we are restricted to consider the cut diagrams, with only (1–2)-particle lines corresponding to the a and j particles [i.e., $\langle 0|\varphi(x)\varphi(y)|0\rangle$ and $\langle \psi(x)\psi(y)\rangle_\beta$, respectively]. The extension of Eq. (2.27) to the case where some external, nonthermalized particles $\{p_k\}$ are present is obvious, and reads

$$\langle T^\dagger \mathcal{P} T\rangle_{\{p_k\},\beta} = i \tilde{\sum_{\text{index}'}} \langle T\rangle_{\{p_k\},\beta}. \tag{2.28}$$

Finally, let us note that using the LTE, one may extend the previous treatment to various Green's functions. The LTE for Green's functions is then a useful starting point for dispersion relations; see, e.g., [1,12].

III. HEAT BATH PARTICLE NUMBER SPECTRUM: GENERAL FRAMEWORK

The cutting equation (2.28) can be fruitfully used for both the partition function Z and the heat bath particle number spectrum $d\langle N(\omega)\rangle/d\omega$ calculations. To see that, let us for simplicity assume that two particles (say, Φ_1,Φ_2) scatter inside a heat bath. We are interested in the heat bath number spectrum after two different particles (say, ϕ_1,ϕ_2) appear in the final state. Except for the condition that the external particles be different from the heat bath ones, no additional assumption about their nature is needed at this stage.

The initial density matrix ρ_i [i.e., the density matrix describing the physical situation before we introduce the particles $\Phi_1(p_1),\Phi_2(p_2)$ into the oven] can be written as

$$\rho_i = Z_i^{-1}\sum_j e^{-\beta K_j}|j;p_1,p_2\rangle\langle j;p_1,p_2|, \tag{3.1}$$

where j denotes the set of occupation numbers for the heat bath particles. A long time after the scattering the final density matrix ρ_f reads

$$\rho_f = Z_f^{-1}\sum_j e^{-\beta K_j}\mathcal{P}S|j;p_1,p_2\rangle\langle j;p_1,p_2|S^\dagger\mathcal{P}^\dagger; \tag{3.2}$$

here, $\mathcal{P}$ is the projection operator projecting out all the nonheat-bath final states except for the $\phi_1(q_1),\phi_2(q_2)$ ones. The S matrix in Eq. (3.2) is defined in a standard way: $S=1+iT$. The Z_f in Eq. (3.2) must be different from Z_i as otherwise ρ_f would not be normalized to unity. In order that ρ_f satisfy the normalization condition $Tr(\rho_f)=1$, one finds

$$Z_f = \sum_j e^{-\beta K_j}\langle j;p_1,p_2|S^\dagger\mathcal{P}S|j;p_1,p_2\rangle = \langle S^\dagger\mathcal{P}S\rangle_{p_1p_2,\beta} Z_i$$
$$= \langle T^\dagger\mathcal{P}T\rangle_{p_1p_2,\beta} Z_i. \tag{3.3}$$

The key point is that we have used in Eq. (3.3) the T matrix because the initial state $|\Phi_1(p_1),\Phi_2(p_2)\rangle$ is, by definition, different from the final one $|\phi(q_1),\phi_2(q_2)\rangle$ and consequently $\mathcal{P}S$ can be replaced by $i\mathcal{P}T$. This allows us to calculate Z_f using directly the diagrammatic technique outlined in the preceding section.

From Eqs. (2.1) and (3.2) one can directly read off that the number spectrum of the heat bath particles is

$$\frac{d\langle N_l(\omega)\rangle_f}{d\omega} = \int \frac{d^3\mathbf{k}}{(2\pi)^3}\delta^+(\omega^2-\mathbf{k}^2-m_l^2) \times\sum_f \langle f|a_l^\dagger(\mathbf{k};\omega)a_l(\mathbf{k};\omega)\rho_f|f\rangle$$
$$= \int \frac{d^3\mathbf{k}}{(2\pi)^3}\delta^+(\omega^2-\mathbf{k}^2-m_l^2) \times\frac{\langle T^\dagger\mathcal{P}a_l^\dagger(\mathbf{k};\omega)a_l(\mathbf{k};\omega)T\rangle_{p_1p_2,\beta}}{\langle T^\dagger\mathcal{P}T\rangle_{p_1p_2,\beta}} \tag{3.4}$$

and, consequently,

$$\langle N_l\rangle_f = \int \frac{d^4k}{(2\pi)^3}\delta^+(k^2-m_l^2)\frac{\langle T^\dagger\mathcal{P}a_l^\dagger(k)a_l(k)T\rangle_{p_1p_2,\beta}}{\langle T^\dagger\mathcal{P}T\rangle_{p_1p_2,\beta}}, \tag{3.5}$$

where we have used the completeness relation for the final states $|f\rangle$ and $[\mathcal{P};a^\dagger a]=0$. The subscript l denotes which type of heat bath particles we are interested in. In the following the index will be mostly suppressed.

IV. MODIFIED CUT DIAGRAMS

To proceed further with Eqs. (3.4) and (3.5), we expand the T matrix in terms of time-ordered interaction-picture fields, i.e.,

$$T[\psi] = \sum_n \int dx_1\cdots\int dx_n\alpha_n(x_1,\ldots,x_n) \times\mathcal{T}[\psi(x_1)\cdots\psi(x_n)]. \tag{4.1}$$

Here ψ represents a heat bath field in the interaction picture. Other fields (i.e., $\bar{\phi}$, ϕ, and Φ) are included in the[4] α_n. An extension of Eq. (4.1) to the case where different heat bath fields are present is natural. Employing Eq. (4.1) in $\langle T^\dagger\mathcal{P}T\rangle_{p_1p_2,\beta}$, one can readily see that this factorizes out in each term of the expansion a *pure* thermal mean value $\langle\cdots\rangle_\beta$. The general structure of each such thermal mean value is $\langle G_m[\psi]F_n[\psi]\rangle_\beta$, where $F_n[\cdots]$ and $G_m[\cdots]$ are the operators with n chronological and m antichronological-time-ordered (heat bath) fields, respectively. Analogous fac-

[4]When Fermi fields are involved, we have, for the sake of compactness, included in the argument of ψ the space-time coordinate, the Dirac index and a discrete index which distinguishes ψ_α from $\bar{\psi}_\alpha$.

torization is true in the expansion of $\langle T^\dagger \mathcal{P}^\dagger a^\dagger a \mathcal{P} T\rangle_{p_1p_2,\beta}$. The only difference is that the pure thermal mean value has the form $\langle G_m[\psi]a^\dagger a F_n[\psi]\rangle_\beta$ instead.[5] In the case when various heat bath fields are present, $m=m_1+m_2+\cdots+m_n$, with m_l denoting the number of the heat bath fields of lth type.

Applying the Dyson-Schwinger equation to $\langle G_m[\psi]a^\dagger a F_n[\psi]\rangle_\beta$ twice and summing over n and m, we get easily the following expression [cf. also Eq. (A11)]:

$$\begin{aligned}\langle T^\dagger \mathcal{P} a_l^\dagger a_l T\rangle_{p_1p_2,\beta} &= \int dxdy\{\langle\psi_l(x)a_l^\dagger\rangle_\beta\langle a_l\psi_l(y)\rangle_\beta+(-1)^p\langle\psi_l(x)a_l\rangle_\beta\langle a_l^\dagger\psi_l(y)\rangle_\beta\}\left\langle \frac{T^\dagger\vec{\delta}}{\delta\psi_l(x)}\,\mathcal{P}\,\frac{\vec{\delta}T}{\delta\psi_l(y)}\right\rangle_{p_1p_2,\beta}\\ &+\int\frac{dxdy}{2}\{\langle\psi_l(x)a_l\rangle_\beta\langle\psi_l(y)a_l^\dagger\rangle_\beta+(-1)^p\langle\psi_l(x)a_l^\dagger\rangle_\beta\langle\psi_l(y)a_l\rangle_\beta\}\left\langle\frac{T^\dagger\vec{\delta}^2}{\delta\psi_l(y)\,\delta\psi_l(x)}\,\mathcal{P}T\right\rangle_{p_1p_2,\beta}\\ &+\int\frac{dxdy}{2}\{\langle a_l\psi_l(x)\rangle_\beta\langle a_l^\dagger\psi_l(y)\rangle_\beta+(-1)^p\langle a_l^\dagger\psi_l(x)\rangle_\beta\langle a_l\psi_l(y)\rangle_\beta\}\left\langle T^\dagger\mathcal{P}\,\frac{\vec{\delta}^2T}{\delta\psi_l(y)\,\delta\psi_l(x)}\right\rangle_{p_1p_2,\beta}\\ &+\langle a_l^\dagger a_l\rangle_\beta\langle T^\dagger\mathcal{P}T\rangle_{p_1p_2,\beta}. \end{aligned}\tag{4.2}$$

A similar decomposition for $\langle T^\dagger\mathcal{P}T\rangle_{p_1p_2,\beta}$ would not be very useful [cf. Eq. (A18)]; instead we define $\langle(T^\dagger\mathcal{P}T)'\rangle_{p_1p_2,\beta}$ having the same expansion as $\langle T^\dagger\mathcal{P}T\rangle_{p_1p_2,\beta}$ except for the $\alpha_n(\cdots)\mathcal{P}\alpha_m^\dagger(\cdots)$ are replaced by $\alpha_n(\cdots)\mathcal{P}\alpha_m^\dagger(\cdots)\,(n_l+m_l)/2$. In this formalism $\langle(T^\dagger\mathcal{P}T)'\rangle_{p_1p_2,\beta}$ is

$$\begin{aligned}\langle(T^\dagger\mathcal{P}T)'\rangle_{p_1p_2,\beta} &= \int dxdy\langle\psi_l(x)\psi_l(y)\rangle_\beta\left\langle\frac{T^\dagger\vec{\delta}}{\delta\psi_l(x)}\,\mathcal{P}\,\frac{\vec{\delta}T}{\delta\psi_l(y)}\right\rangle_{p_1p_2,\beta}\\ &+\int\frac{dxdy}{2}\langle\overline{\mathcal{T}}[\psi_l(x)\psi_l(y)]\rangle_\beta\left\langle\frac{T^\dagger\vec{\delta}^2}{\delta\psi_l(y)\,\delta\psi_l(x)}\,\mathcal{P}T\right\rangle_{p_1p_2,\beta}\\ &+\int\frac{dxdy}{2}\langle\mathcal{T}[\psi_l(x)\psi_l(y)]\rangle_\beta\left\langle T^\dagger\mathcal{P}\,\frac{\vec{\delta}^2T}{\delta\psi_l(y)\,\delta\psi_l(x)}\right\rangle_{p_1p_2,\beta},\end{aligned}\tag{4.3}$$

with the $\overline{\mathcal{T}}$ being the antichronological ordering symbol. Comparing Eq. (4.3) with Eq. (A19), we can interpret the RHS of Eq. (4.3) as a sum over *all* possible distributions of one line (corresponding to ψ_l) inside of each given ($T\neq0$) cut diagram constructed out of $\langle T^\dagger\mathcal{P}T\rangle_{p_1p_2,\beta}$. As Eq. (4.3) has precisely the same diagrammatical structure as $\langle T^\dagger\mathcal{P}a^\dagger aT\rangle_{p_1p_2,\beta}-\langle a^\dagger a\rangle_\beta\langle T^\dagger\mathcal{P}T\rangle_{p_1p_2,\beta}$ [cf. Eq. (4.2)], it shows that in order to compute the numerator of[6] $d\Delta\langle N(\omega)\rangle/d\omega=d\langle N(\omega)\rangle_f/d\omega-d\langle N(\omega)\rangle_i/d\omega$ one can simply modify the usual $\langle T^\dagger\mathcal{P}T\rangle_{p_1p_2,\beta}$ cut diagrams by the following one-line replacements [cf. Eq. (3.4)].

(i) For *neutral scalar bosons*,

$$\begin{aligned}\langle\varphi(x)\varphi(y)\rangle_\beta &\to \int\frac{d^3\mathbf{k}}{(2\pi)^3}\,\delta^+(\omega^2-\mathbf{k}^2-m^2)\{\langle\varphi(x)a^\dagger(\mathbf{k};\omega)\rangle_\beta\langle a(\mathbf{k};\omega)\varphi(y)\rangle_\beta+\langle\varphi(x)a(\mathbf{k};\omega)\rangle_\beta\langle a^\dagger(\mathbf{k};\omega)\varphi(y)\rangle_\beta\}\\ &=\int\frac{d^4k}{(2\pi)^3}\,\delta(k^2-m^2)\{f_B(\omega)[f_B(\omega)+1][\delta^-(k_0+\omega)+\delta^+(k_0-\omega)]+\delta^+(k_0-\omega)[1+f_B(\omega)]\\ &\quad-\delta^-(k_0+\omega)f_B(\omega)\}e^{-ik(x-y)},\end{aligned}\tag{4.4}$$

where $f_B(\omega)$ is the Bose-Einstein distribution: $f_B(\omega)=1/(e^{\beta|\omega|}-1)$. The term $\theta(-k_0)f_B(\omega)$ describes the absorption of a heat bath particle, and so reduces the number spectrum: that is why the negative sign appears in front of it. Analogously,

$$\langle\mathcal{T}[\varphi(x)\varphi(y)]\rangle_\beta\to\int\frac{d^3\mathbf{k}}{(2\pi)^3}\,\delta^+(\omega^2-\mathbf{k}^2-m^2)\{\langle a^\dagger(\mathbf{k};\omega)\varphi(x)\rangle_\beta\langle a(\mathbf{k};\omega)\varphi(y)\rangle_\beta+\langle a(\mathbf{k};\omega)\varphi(x)\rangle_\beta\langle a^\dagger(\mathbf{k};\omega)\varphi(y)\rangle_\beta\}$$

[5]Remember that $\mathcal{P}=\mathcal{P}'\otimes\mathcal{P}''=|q_1,q_2\rangle\langle q_1,q_2|\otimes\Sigma_j|j\rangle\langle j|$. Here $\mathcal{P}''=\Sigma_j|j\rangle\langle j|$ behaves as an identity in the subspace of heat bath states.

[6]Here $d\langle N(\omega)\rangle_i/d\omega=\int[d^3\mathbf{k}/(2\pi)^3]\,\delta^+(\omega^2-\mathbf{k}^2-m^2)\langle a^\dagger(\omega,\mathbf{k})a(\omega,\mathbf{k})\rangle_\beta$ [cf. Eq. (3.4)].

$$= \int \frac{d^4k}{(2\pi)^3}\,\delta(k^2-m^2)[1+f_B(\omega)]f_B(\omega)e^{-ik(x-y)}[\,\delta^+(k_0-\omega)+\delta^-(k_0+\omega)]. \tag{4.5}$$

Similarly, for $\Delta\langle N\rangle$ one needs the following replacements [cf. Eq. (3.5)]:

$$\langle\varphi(x)\varphi(y)\rangle_\beta \to \int \frac{d^4k}{(2\pi)^3}\,\delta(k^2-m^2)\{f_B(\omega_k)[f_B(\omega_k)+1]+\theta(k_0)[1+f_B(\omega_k)]-\theta(-k_0)f_B(\omega_k)\}e^{-ik(x-y)},$$

$$\langle\mathcal{T}[\varphi(x)\varphi(y)]\rangle_\beta \to \int \frac{d^4k}{(2\pi)^3}\,\delta(k^2-m^2)[1+f_B(\omega_k)]f_B(\omega_k)e^{-ik(x-y)}, \tag{4.6}$$

with $\omega_k=\sqrt{\mathbf{k}^2-m^2}$.

(ii) For *Dirac fermions*, the Dirac field is comprised of two different types of excitations (mutually connected via charge conjugation), and so the corresponding number operator $N(\omega)=N_b(\omega)+N_d(\omega)$, with

$$N_b(\omega)=\sum_{\alpha=1,2}\int \frac{d^3\mathbf{k}}{(2\pi)^3}\,\delta^+(\omega^2-\mathbf{k}^2-m^2)b^\dagger_\alpha(\mathbf{k};\omega)b_\alpha(\mathbf{k};\omega),$$

$$N_d(\omega)=\sum_{\alpha=1,2}\int \frac{d^3\mathbf{k}}{(2\pi)^3}\,\delta^+(\omega^2-\mathbf{k}^2-m^2)d^\dagger_\alpha(\mathbf{k};\omega)d_\alpha(\mathbf{k};\omega).$$

Thus, the one-line replacements needed for $d\Delta\langle N_b(\omega)\rangle/d\omega$ are

$$\begin{aligned}\langle\psi_\rho(x)\bar\psi_\sigma(y)\rangle_\beta \to \sum_{\alpha=1,2}\int \frac{d^3\mathbf{k}}{(2\pi)^3}\,\delta^+(\omega^2-\mathbf{k}^2-m^2)\{&\langle\psi_\rho(x)b^\dagger_\alpha(\mathbf{k};\omega)\rangle_\beta\langle b_\alpha(\mathbf{k};\omega)\bar\psi_\sigma(y)\rangle_\beta\\ &-\langle\psi_\rho(x)b_\alpha(\mathbf{k};\omega)\rangle_\beta\langle b^\dagger_\alpha(\mathbf{k};\omega)\bar\psi_\sigma(y)\rangle_\beta\}\\ =\int \frac{d^4k}{(2\pi)^3}\,\delta^+(k^2-m^2)\,\delta(k_0-\omega)(\not k+m)_{\rho\sigma}&\{[1-f_F(\omega)]-f_F(\omega)[1-f_F(\omega)]\}e^{-ik(x-y)},\end{aligned} \tag{4.7}$$

where $f_F(\omega)$ is the Fermi-Dirac distribution, $f_F(\omega)=1/e^{\beta(|\omega|-\mu)}+1$, and

$$\begin{aligned}\langle\mathcal{T}[\psi_\rho(x)\bar\psi_\sigma(y)]\rangle_\beta \to \sum_{\alpha=1,2}\int \frac{d^3\mathbf{k}}{(2\pi)^3}\,\delta^+(\omega^2-\mathbf{k}^2-m^2)\{&\langle b_\alpha(\mathbf{k};\omega)\psi_\rho(x)\rangle_\beta\langle b^\dagger_\alpha(\mathbf{k};\omega)\bar\psi_\sigma(y)\rangle_\beta\\ &-\langle b^\dagger_\alpha(\mathbf{k};\omega)\psi_\rho(x)\rangle_\beta\langle b_\alpha(\mathbf{k};\omega)\bar\psi_\sigma(y)\rangle_\beta\}\\ =-\int \frac{d^4k}{(2\pi)^3}\,\delta^+(k^2-m^2)\,\delta(k_0-\omega)(\not k+m)_{\rho\sigma}&f_F(\omega)[1-f_F(\omega)]e^{-ik(x-y)}.\end{aligned} \tag{4.8}$$

Correspondingly, for $\Delta\langle N_b\rangle$ we need

$$\langle\psi_\rho(x)\bar\psi_\sigma(y)\rangle_\beta \to \int \frac{d^4k}{(2\pi)^3}\,\delta^+(k^2-m^2)(\not k+m)_{\rho\sigma}\{[1-f_F(\omega)]-f_F(\omega)[1-f_F(\omega)]\}e^{-ik(x-y)},$$

$$\langle\mathcal{T}[\psi_\rho(x)\bar\psi_\sigma(y)]\rangle_\beta \to -\int \frac{d^4k}{(2\pi)^3}\,\delta^+(k^2-m^2)(\not k+m)_{\rho\sigma}f_F(\omega)[1-f_F(\omega)]e^{-ik(x-y)}. \tag{4.9}$$

For the d-type excitations the prescription is very similar. Actually, in order to get $d\Delta\langle N_d(\omega)\rangle/d\omega$, the following substitutions must be performed in Eqs. (4.7)–(4.9): $\theta(k_0)\to\theta(-k_0)$, $f_F\to(1-f_F)$, and $\mu\to-\mu$.

(iii) For *gauge fields in the axial temporal gauge ($A^0=0$)*, the temporal gauge is generally incorporated in the gauge fixing sector of the Lagrangian and particularly

$$\mathcal{L}_{\rm fix}=-\frac{1}{2\alpha}(A_0)^2, \quad \alpha\to 0. \tag{4.10}$$

The principal advantage of the axial gauges arises from the decoupling the FP ghosts in the theory. This statement is of course trivial in QED as any linear gauge (both for covariant and noncovariant cases) brings this decoupling automatically [1]. A particular advantage of the temporal gauge comes from an elimination of nonphysical scalar photons from the very beginning.

Let us decompose a gauge field A_i, $i=1,2,3$, into the transverse and longitudial parts, i.e., $A_i=A^T_i+A^L_i$, with

$$A_i^T=\left(\delta_{ij}-\frac{\partial_i\partial_j}{\vec{\partial}^2}\right)A_j \quad \text{and} \quad A_i^L=\frac{\partial_i\partial_j}{\vec{\partial}^2}A_j\,, \tag{4.11}$$

and use the sum over gauge-particle polarizations,

$$\sum_{\lambda=1}^{2}\varepsilon_i^{(\lambda)}(k)\varepsilon_j^{(\lambda)}(k)=\delta_{ij}-\frac{k_ik_j}{\mathbf{k}^2}, \tag{4.12}$$

with $\varepsilon^{(\lambda)}(k)$ being polarization vectors; then, for $d\Delta\langle N^T(\omega)\rangle/d\omega$ we get the following one-line replacements:

$$\begin{aligned}\langle A_i^T(x)A_j^T(y)\rangle_\beta \rightarrow &\sum_{\lambda=1}^{2}\int\frac{d^3\mathbf{k}}{(2\pi)^3}\delta^+(\omega^2-\mathbf{k}^2-m^2)\langle A_i^T(x)a_\lambda^\dagger(\mathbf{k};\omega)\rangle_\beta\langle a_\lambda(\mathbf{k};\omega)A_j^T(y)\rangle_\beta\\ &+\langle A_i^T(x)a_\lambda(\mathbf{k};\omega)\rangle_\beta\langle a_\lambda^\dagger(\mathbf{k};\omega)A_j^T(y)\rangle_\beta\}\\ =&\left(\delta_{ij}-\frac{\partial_i\partial_j}{\vec{\partial}^2}\right)\quad[\text{Eq. (4.4)}],\end{aligned}$$

$$\begin{aligned}\langle\mathcal{T}[A_i^T(x)A_j^T(y)]\rangle_\beta \rightarrow &\sum_{\lambda=1}^{2}\int\frac{d^3\mathbf{k}}{(2\pi)^3}\delta^+(\omega^2-\mathbf{k}^2-m^2)\langle A_i^T(x)a_\lambda^\dagger(\mathbf{k};\omega)\rangle_\beta\langle A_i^T(y)a_\lambda(\mathbf{k};\omega)\rangle_\beta\\ &+\langle A_i^T(x)a_\lambda(\mathbf{k};\omega)\rangle_\beta\langle A_i^T(x)a_\lambda^\dagger(\mathbf{k};\omega)\rangle_\beta\\ =&\left(\delta_{ij}-\frac{\partial_i\partial_j}{\vec{\partial}^2}\right)\quad[\text{Eq. (4.5)}].\end{aligned} \tag{4.13}$$

The replacements needed for $\Delta\langle N^T\rangle$ can be concisely expressed as

$$\langle\cdots\rangle_\beta\rightarrow\left(\delta_{ij}-\frac{\partial_i\partial_j}{\vec{\partial}^2}\right)\quad[\text{Eq. (4.6)}]. \tag{4.14}$$

As for the longitudial (nonphysical) degrees of freedom, it is obvious that

$$\langle A_i^L(x)A_j^L(y)\rangle_\beta\,,\quad\langle\mathcal{T}[A_i^L(x)A_j^L(y)]\rangle_\beta\rightarrow 0. \tag{4.15}$$

Equations (4.4)–(4.14) can be most easily derived in the finite-volume limit; e.g., for a scalar field we reformulate $\varphi(x)$ as

$$\varphi(x)=\sum_r\frac{A_r}{\sqrt{2E_rV}}e^{-iE_rt+i\mathbf{k}_r\mathbf{x}}+\frac{A_r^\dagger}{\sqrt{2E_rV}}e^{iE_rt-i\mathbf{k}_r\mathbf{x}},$$

rescaling the annihilation and creation operators by defining $a(k)=\sqrt{2E_kV}A_k$ in such a way that $[A_k;A_{k'}^\dagger]=\delta_{kk'}$ [so that $\langle A_k^\dagger A_{k'}\rangle_\beta=\delta_{kk'}f_B(k_0)$], while $\int d^3\mathbf{k}/(2\pi)^3\rightarrow(1/V)\,\Sigma_{\mathbf{k}}$.

The replacements (4.4)–(4.15) are meant in the following sense: First, one constructs all the $T\neq 0$ diagrams for $\langle T^\dagger\mathcal{P}T\rangle_{p_1p_2,\beta}$, using the LTE (2.28) and the rules mentioned therein. In order to calculate the numerator of Eqs. (3.4) or (3.5) we simply replace (using corresponding prescriptions) *one* heat bath particle line in each cut diagram and this replacement must sum for all the possible heat bath particle lines in the diagram. If more types of heat bath particles are present, we replace only those lines which correspond to particles whose number spectrum we want to compute (see Fig. 6).

The terms in the replacements (4.4)–(4.14) have a direct physical interpretation. The $f(\omega_k)$ and $[1+(-1)^pf(\omega_k)]$ can be viewied as the absorption and emission of the heat bath particles, respectively [3]. The term $f(\omega_k)[1+(-1)^pf(\omega_k)]$ describes the fluctuations of the heat bath particles. This is because for the noninteracting heat bath particles $\langle(n_k-\langle n_k\rangle_\beta)^2\rangle_\beta=f(\omega_k)[1+(-1)^pf(\omega_k)]$. The substituted propagators can be therefore schematically depicted as

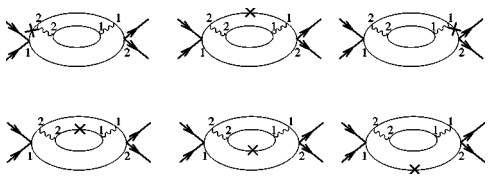

FIG. 6. The numerator of Eqs. (3.4) and (3.5) can be calculated using the modified cut diagrams for $\langle T^\dagger\mathcal{P}T\rangle_{p_1p_2,\beta}$. As an example we depict all the possible contributions to the numerator derived from the cut diagram on Fig. 4(c). The wavy lines and thin lines describe the heat bath particles. The crossed lines denote the substituted propagators; in this case we wish to calculate the thin-line particle number spectrum.

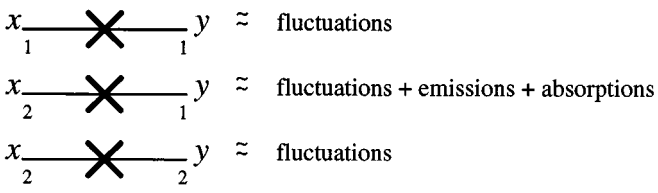

Collecting all the contributions from emissions, absorptions, and fluctuations separately, one can schematically write

$$\frac{d\langle N(\omega)\rangle_f}{d\omega}=\frac{d\langle N(\omega)\rangle_i}{d\omega}+F^{\text{emission}}(\omega)+F^{\text{absorption}}(\omega)+F^{\text{fluc}}(\omega), \tag{4.16}$$

where, for instance, for neutral scalar bosons,

$$F^{\text{emission}}(\omega)=Z_f^{-1}\int\frac{d^4k}{(2\pi)^3}\,\delta^+(k^2-m^2)\,\delta(k_0-\omega)\times[1+f_B(\omega)]\left\langle\frac{T^\dagger\vec{\delta}}{\delta\psi(x)}\,\mathcal{P}\,\frac{\vec{\delta}T}{\delta\psi(y)}\right\rangle_{p_1p_2,\beta}.$$

Using Eq. (4.5), it is easy to write down analogous expressions for $F^{\text{absorption}}$ and F^{fluc}. To the lowest perturbative order, the form (4.16) was obtained by Landshoff and Taylor [3].

V. MODEL PROCESS

A. Basic assumptions

To illustrate the modified cut diagram technique, we shall restrict ourselves to a toy model, namely, to a scattering of two neutral scalar particles Φ (pions) within a photon heat bath, with a pair of scalar charged particles $\phi,\bar{\phi}$ (''muon'' and ''antimuon'') left as a final product. Both initial and final particles are supposed to be unheated. We further assume that the heat bath photons A are scalars; i.e., the heat bath Hamiltonian has the form

$$H^{hb}=\frac{1}{2}(\partial_\nu A)^2-\frac{m_\gamma^2}{2}A^2.$$

In order to mimic the scalar electrodynamic, we have chosen the interacting Hamiltonian entering in the T matrix as

$$H_{\text{in}}=\frac{\lambda}{2}\Phi^2\phi\phi^\dagger+\left(eA+\frac{e^2}{2}A^2\right)\phi\phi^\dagger.$$

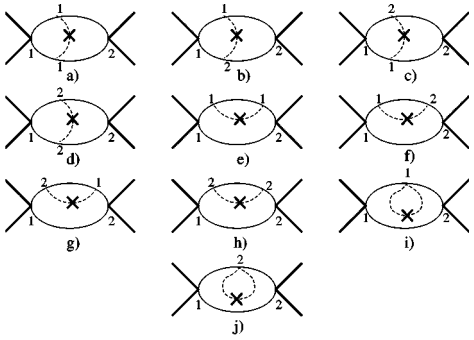

FIG. 7. The modified cut diagrams involved in an order-e^2 contribution to the photon number spectrum. Dashed lines: photons. Solid lines: ϕ, $\phi^\dagger$ particles. Bold lines: Φ particles.

B. Calculations

We can now compute an order-e^2 contribution to the $d\Delta\langle N_\gamma(\omega)\rangle/d\omega$. The evaluation of the $d\Delta\langle N_\gamma(\omega)\rangle/d\omega$ is straightforward. In Fig. 7 we list all the modified cut diagrams contributing to an order e^2.

Note that diagrams (b) and (c) are topologically identical. Similarly, diagrams (e), (f), (h), (i), and (j) should be taken with combinatorial factor of 2 (corresponding diagrams with a heat bath particle line on the bottom solid line are not shown). Of course, diagram (g) vanishes for kinematic reasons. For instance, in order to calculate the contribution from diagram (a) (see also Fig. 8) we go back to Eq. (2.9) and to prescriptions (4.4) and (4.5), so we get

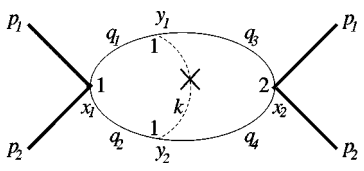

FIG. 8. The diagram (a) with a corresponding kinematics.

$$
\begin{aligned}
(\mathrm{a}) &= \frac{-\lambda^2 e^2}{V^2 4\omega_{p_1}\omega_{p_2}} \int d^4x_1 d^4x_2 d^4y_1 d^4y_2 e^{-i(p_1+p_2)x_1} e^{i(p_1+p_2)x_2} i\Delta_F(y_1-x_1) i\Delta_F(y_2-x_1) \\
&\quad \times i\Delta^-(y_1-x_2) i\Delta^-(y_2-x_2) \int \frac{d^4k}{(2\pi)^3} \delta(k^2-m^2)[1+f_B(\omega)] f_B(\omega)[\delta^+(k_0-\omega)+\delta^-(k_0+\omega)] e^{-ik(y_1-y_2)} \\
&= \frac{\lambda^2 e^2 t}{V 4\omega_{p_1}\omega_{p_2}(2\pi)^5} f_B(\omega)[1+f_B(\omega)] \int d^4k d^4q_3 d^4q_4 \delta^+(q_3^2-m_\mu^2)\delta^+(q_4^2-m_\mu^2) \\
&\quad \times \delta(k_0-\omega)\left\{ \frac{1}{-2q_3k+m_\gamma^2}\frac{1}{2q_4k+m_\gamma^2} + \frac{1}{2q_3k+m_\gamma^2}\frac{1}{-2q_4k+m_\gamma^2} \right\} \delta(k^2-m_\gamma^2)\delta^4(-p_1-p_2+q_1+q_2). \qquad (5.1)
\end{aligned}
$$

We have dropped the $i\varepsilon$ prescription in the propagators since adding (subtracting) an on-shell momenta $q_{1;2}$ to (from) an on-shell momenta k we cannot fulfill the condition $(k\pm q_{1;2})^2=m_\mu^2$. As is usual, we have assumed that our interaction is enclosed in a ''time'' and volume box (t and V, respectively). Analogously one can calculate contributions from other diagrams in Fig. 7. Let us emphasize that it is necessary to give sense to graphs (e), (h), (i), and (j) as these suffer with the pinch singularity; the muon-particle propagator $(p_{1;2}^2-m^2)^{-1}$ has to be evaluated at its pole because of the presence of an on-shell line (1–2 line) with the same momenta. Some regularization is obviously necessary. Using the formal identity [1]

$$
\frac{1}{x\pm i\varepsilon}\delta(x) = -\frac{1}{2}\delta'(x) \mp i\pi[\delta(x)]^2, \qquad (5.2)
$$

we discover that the unwanted δ^2 mutually cancel between (e) and (h) diagrams [similarly for (i) and (j) diagrams]. An alternative (but lengthier) way of dealing with the latter pinch singularity, i.e., switching off the interaction with a heat bath in the remote past and future, is discussed in [14]. Evaluating all the diagrams (note that we should attach to each diagram the factor of 1/2! coming from a Taylor expansion of the T matrix), we are left with [c.f. Eq. (4.16)]

$$
\begin{aligned}
F^{\text{emission}}(\omega)+F^{\text{absorption}}(\omega) &= \frac{t\lambda^2 e^2}{\langle T\mathcal{P}T^\dagger\rangle_{p_1p_2,\beta} V 8\omega_{p_1}\omega_{p_2}(2\pi)^5} \int d^4k\,\delta(k^2-m_\gamma^2)\delta(k_0-\omega)\int d^4q_1 d^4q_2 \delta^+(q_1^2-m_\mu^2) \\
&\quad \times \delta^+(q_2^2-m_\mu^2)\{K_1[1+f_B(\omega)]\delta^4(-Q+q_1+q_2+k)-K_2 f_B(\omega)\delta^4(-Q+q_1+q_2-k)\} \qquad (5.3)
\end{aligned}
$$

and

$$
\begin{aligned}
F^{\text{fluct}}(\omega) &= \frac{t\lambda^2 e^2 f_B(\omega)[1+f_B(\omega)]}{\langle T\mathcal{P}T^\dagger\rangle_{p_1p_2,\beta} V 8\omega_{p_1}\omega_{p_2}(2\pi)^5} \int d^4k\,\delta(k^2-m_\gamma^2)\delta(k_0-\omega)\int d^4q_1 d^4q_2 \delta^+(q_1^2-m_\mu^2)\delta^+(q_2^2-m_\mu^2) \\
&\quad \times\{\delta^4(-Q+q_1+q_2+k)K_1+\delta^4(-Q+q_1+q_2-k)K_2-2\,\delta^4(-Q+q_1+q_2)K_3\} \\
&\quad + \frac{t\lambda^2 e^2 f_B(\omega)[1+f_B(\omega)]}{\langle T\mathcal{P}T^\dagger\rangle_{p_1p_2,\beta} V 8\omega_{p_1}\omega_{p_2}(2\pi)^5} \int d^4k\,\delta(k^2-m_\gamma^2)\delta(k_0-\omega)\int d^4q_1 d^4q_2 \delta^4(-Q+q_1+q_2) \\
&\quad \times\left\{\left(1-\frac{1}{2q_1k-m_\gamma^2}+\frac{1}{2q_1k+m_\gamma^2}\right)\delta^+(q_2^2-m_\mu^2)\,\frac{\partial}{\partial m_\mu^2}\delta^+(q_1^2-m_\mu^2)+(q_1\leftrightarrow q_2)\right\} \qquad (5.4)
\end{aligned}
$$

with $K_1=(1/2q_1k+m_\gamma^2+1/2q_2k+m_\gamma^2)^2$, $K_2=(1/2q_1k-m_\gamma^2+1/2q_2k-m_\gamma^2)^2$, $K_3=2/(2q_1k-m_\gamma^2)(2q_2k+m_\gamma^2)$, and $Q=p_1+p_2$. The relevant [i.e., order-e^0 (see Fig. 9)] term for $\langle T\mathcal{P}T^\dagger\rangle_{p_1p_2,\beta}$ reads

$$
\begin{aligned}
\langle T\mathcal{P}T^\dagger\rangle_{p_1p_2,\beta} &= \frac{\lambda^2 t}{16V\omega_{p_1}\omega_{p_2}(2\pi)^2}\int d^4q_1 d^4q_2 \delta^+(q_1^2-m_\mu^2)\delta^+(q_2^2-m_\mu^2)\delta^4(-Q+q_1+q_2) \\
&= \frac{\lambda^2 t}{64V\omega_{p_1}\omega_{p_2}|Q|(2\pi)}\sqrt{Q^2-4m_\mu^2}. \qquad (5.5)
\end{aligned}
$$

Equations (5.3) and (5.4) are analogous to the result obtained in [3] for the decay. In order to understand their structure, let us deal with the number spectrum for small[7] ω's. To do this, we change the integration variables

$$q_1 \to q_1 \mp \frac{1}{2}k,$$

$$q_2 \to q_2 \mp \frac{1}{2}k. \tag{5.6}$$

These changes lead to

$$(2q_i k \pm m_\gamma^2)\,\delta^+(q_1^2-m_\mu^2)\,\delta^+(q_2-m_\mu^2)\,\delta^4(-Q+q_1+q_2\pm k)$$
$$\to 2q_i k\,\delta^+(q_1^2-M^2\mp X)\,\delta^+(q_2^2-M^2\mp Y)$$
$$\times\,\delta^4(-Q+q_1+q_2), \tag{5.7}$$

where $M^2=m_\mu^2-\frac{1}{4}m_\gamma^2$, $X=q_1k$, and $Y=q_2k$. In addition, transformations (5.6) have unite Jacobian. If one Taylor expands Eq. (5.7) in terms of X and Y, then one gets successively higher ω contributions to Eqs. (5.3) and (5.4). Expanding Eq. (5.3) to the first order in X and Y, and keeping only temperature-dependent pieces, we have

$$\langle T\mathcal{P}T^\dagger\rangle_{p_1p_2,\beta}\frac{8V\omega_{p_1}\omega_{p_2}}{t}[F^{\text{emission}}(\omega)+F^{\text{absorption}}(\omega)]$$
$$\sim\frac{\lambda^2e^2}{(2\pi)^5}f_B(\omega)\int d^4q_1d^4q_2\,\delta(k^2-m_\gamma^2)\,\delta(k_0-\omega)A, \tag{5.8}$$

with

$$A=\frac{\partial}{\partial_{M_1^2}}\int d^4q_1d^4q_2\,\delta^+(q_1^2-M_1^2)\,\delta^+(q_2^2-M_2^2)(4KX)$$
$$\times\,\delta^4(Q-q_1-q_2)|_{M_1=M_2=M}.$$

Here $K=(1/2q_1k+1/2q_2k)^2$ [we have performed transformation $q_1\leftrightarrow q_2$ in order to express Eq. (5.8) solely in terms of X]. As A is a Lorentz scalar, it must depend on k only via product (kQ). One can thus evaluate A in the frame where $Q=(Q_0,\mathbf{0})$ and then replace ωQ_0 by (kQ) (see also [3]). Straightforward calculations show that

$$A=\frac{-(2\pi)(kQ)^3}{|Q|\sqrt{\frac{Q^2}{4}-M^2}\left[\frac{M}{|Q|}(kQ)^2+m_\gamma^2\left(\frac{|Q|^3}{4}-MQ^2\right)\right]^2}. \tag{5.9}$$

Recalling Eq. (5.5), we get

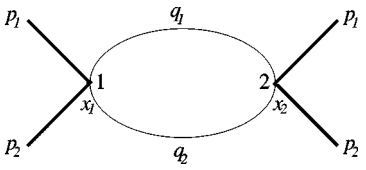

FIG. 9. The lowest-order cut diagram for $\langle T\mathcal{P}T^\dagger\rangle_{p_1p_2,\beta}$.

$$F^{\text{emission}}(\omega)+F^{\text{absorption}}(\omega)$$
$$\sim\frac{Q^2f_B(\omega)e^2}{\pi^2M^2\sqrt{Q_0^2-Q^2}\sqrt{Q^2-4M^2}\sqrt{Q^2-4m_\mu^2}}$$
$$\times\left\{\ln\left(\frac{(\omega Q_0+|\mathbf{k}||\mathbf{Q}|)^2+m_\gamma^2\frac{Q^2}{M^2}\left(\frac{Q^2}{4}-M^2\right)}{(\omega Q_0-|\mathbf{k}||\mathbf{Q}|)^2+m_\gamma^2\frac{Q^2}{M^2}\left(\frac{Q^2}{4}-M^2\right)}\right)\right.$$
$$+\frac{m_\gamma^2\left(\frac{Q^2}{4}-M^2\right)}{\frac{M^2}{Q^2}(\omega Q_0-|\mathbf{k}||\mathbf{Q}|)^2+m_\gamma^2\left(\frac{Q^2}{4}-M^2\right)}$$
$$\left.-\frac{m_\gamma^2\left(\frac{Q^2}{4}-M^2\right)}{\frac{M^2}{Q^2}(\omega Q_0+|\mathbf{k}||\mathbf{Q}|)^2+m_\gamma^2\left(\frac{Q^2}{4}-M^2\right)}\right\} \tag{5.10}$$

with $|\mathbf{k}|=\sqrt{\omega^2-m_\gamma^2}$ and $|\mathbf{Q}|=\sqrt{Q_0^2-Q^2}$. Equation (5.10) takes a particularly simple form if m_γ is negligibly small (i.e., if $m_\gamma\ll\omega$); then,

$$F^{\text{emission}}(\omega)+F^{\text{absorption}}(\omega)$$
$$\sim\frac{2f_B(\omega)e^2}{\pi^2}\frac{Q^2}{m_\mu^2\sqrt{Q_0^2-Q^2}(Q^2-4m_\mu^2)}$$
$$\times\ln\left(\frac{Q_0+\sqrt{Q_0^2-Q^2}}{Q_0-\sqrt{Q_0^2-Q^2}}\right). \tag{5.11}$$

For small ω one may replace $f_B(\omega)$ by $\beta\omega$. As a result, the leading behavior of $F^{\text{emission}}+F^{\text{absorption}}$ for small ω goes like ω^{-1}, provided $m_\gamma\ll\omega$. Let us mention that parts proportional to ω^{-2} have mutually canceled in the zeroth order of a Taylor expansion.

Similarly as in the previous case we can evaluate F^{fluct}. Performing transformation (5.6), and expanding Eq. (5.4) to the first order in X and Y, we get

[7]So we implicitly assume that the photon mass m_γ is sufficiently small.

$$\langle T\mathcal{P}T^{\dagger}\rangle_{p_1p_2,\beta}\frac{8V\omega_{p_1}\omega_{p_2}}{t}F^{\rm fluct}(\omega)$$

$$\sim\frac{\lambda^2e^2}{(2\pi)^5}f_B(\omega)[1+f_B(\omega)]$$

$$\times\int d^4q_1d^4q_2\delta(k^2-m_\gamma^2)\delta(k_0-\omega)B, \tag{5.12}$$

with

$$B=\int d^4q_1d^4q_2\delta^4(Q-q_1-q_2)\left(\frac{\partial}{\partial m_\mu^2}\right)\delta^+(q_1^2-m_\mu^2)$$

$$\times\delta^+(q_2^2-m_\mu^2)+\int d^4q_1d^4q_2\delta^4(Q-q_1-q_2)$$

$$\times\left\{\left(\frac{\partial}{\partial M}\right)^2-2\left(\frac{Qk}{q_1k}\right)\frac{\partial^2}{\partial M_1\partial M_2}\right\}$$

$$\times\delta^+(q_1^2-M_1^2)\delta^+(q_2^2-M_2^2)|_{M_1=M_2=M}.$$

Direct calculations lead to

$$B=\frac{2\pi(kQ)^2}{Q^2(Q^2-4M^2)^{3/2}}\left\{\frac{M^2}{\left[\frac{M^2}{Q^2}(kQ)^2+m_\gamma^2\left(\frac{Q^2}{4}-M^2\right)\right]}-\frac{\left(\frac{Q^2}{4}-M^2\right)(2M^2-Q^2)m_\gamma^2}{\left[\frac{M^2}{Q^2}(kQ)^2+m_\gamma^2\left(\frac{Q^2}{4}-M^2\right)\right]^2}\right\}$$

$$-\frac{\pi}{|Q|\sqrt{Q^2-4M^2}}-\frac{2\pi}{|Q|(Q^2-4M^2)^{3/2}}.$$

After some analysis we finally get

$$F^{\rm fluct}(\omega)\sim\frac{f_B(\omega)[1+f_B(\omega)]m_\gamma e^2}{4\pi^2M^2\sqrt{Q_0^2-Q^2}\sqrt{Q^2-4m_\mu^2}}\left\{\frac{|Q|}{M}\left[\text{arctg}\left(\frac{\frac{M}{|Q|}(\omega Q_0+|\mathbf{k}||\mathbf{Q}|)}{m_\gamma\sqrt{\frac{Q^2}{4}-M^2}}\right)-\text{arctg}\left(\frac{\frac{M}{|Q|}(\omega Q_0-|\mathbf{k}||\mathbf{Q}|)}{m_\gamma\sqrt{\frac{Q^2}{4}-M^2}}\right)\right]\right.$$

$$\left.+\frac{(2M^2-Q^2)m_\gamma}{2\sqrt{Q^2-4M^2}}\left[\frac{\omega Q_0+|\mathbf{k}||\mathbf{Q}|}{\frac{M^2}{Q^2}(\omega Q_0+|\mathbf{k}||\mathbf{Q}|)^2+m_\gamma^2\left(\frac{Q^2}{4}-M^2\right)}-\frac{\omega Q_0-|\mathbf{k}||\mathbf{Q}|}{\frac{M^2}{Q^2}(\omega Q_0-|\mathbf{k}||\mathbf{Q}|)^2+m_\gamma^2\left(\frac{Q^2}{4}-M^2\right)}\right]\right\}$$

$$-\frac{f_B(\omega)[1+f_B(\omega)]|\mathbf{k}|e^2}{\pi^2(Q^2-4m_\mu^2)}. \tag{5.13}$$

Expression (5.13) considerably simplifies in the limit $m_\gamma\to0$. In the latter case

$$F^{\rm fluct}\sim-\frac{f_B(\omega)[1+f_B(\omega)]\omega e^2}{\pi^2(Q^2-4m_\mu^2)}, \tag{5.14}$$

and so the leading behavior for $F^{\rm fluct}$ at small ω and $m_\gamma\ll\omega$ is dominated by ω^{-1}. Note that separate contributions to the zeroth order of a Taylor expansion of $F^{\rm fluc}$ behave as ω^{-2} but they cancel between themselves, leaving behind parts proportional at worst to ω^{-1}. The minus sign in Eq. (5.14) reflects the fact that the fluctuations tend to suppress an increase in the particle number spectrum when ω is small. On the other hand, from Eq. (5.11) we see that the emissions and absorptions stimulate an increase in the particle number spectrum for small ω.

A result similar to Eqs. (5.11) and (5.14) has been derived by Landshoff and Taylor [3] for a decay using proper scalar electrodynamics, though in their case a contribution from the emission and absorption dominated over fluctuations for small ω. Note that in our model both contributions are of comparable size at $\omega\sim0$. The former feature is inherently connected with the fact that our ''photons'' are scalar particles. If photons were vector particles, an additional photon momentum k_μ would go with each three-line photon-muon vertex and so one might expect that the contributions (5.11) and (5.14) would ''soften'' at small ω. We have checked explicitly that for zero-mass photons in the axial temporal gauge (i.e., $A^0=0$) this is indeed the case, and it was found that $F^{\rm emission}+F^{\rm absorption}\propto\omega^{-1}$ while $F^{\rm fluct}\propto\omega$.

Until now we have supposed that our heat bath contains only (scalar) photons in thermal equilibrium. However, one could similarly treat a heat bath which is comprised of pho-

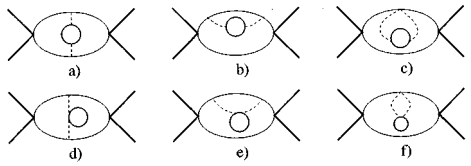

FIG. 10. The generating thermal diagrams involved in an order-e^4 contribution to the electron number spectrum. Dashed lines: photons. Thin lines: ϕ, $\phi^\dagger$ particles. Bold lines: Φ particles. Half-bold lines: electrons.

tons and charged particles, let us say electrons, mutually coexisting in thermal equilibrium. To be more specific, let us assume that the heat bath photons A and electrons Ψ are both scalars so the heat bath Hamiltonian takes the form

$$H^{hb}=H^{\gamma}+H^{e}+eA\Psi\Psi^{\dagger}+\frac{e^2}{2}A^2\Psi\Psi^{\dagger},$$

$$H^{e}=\partial_{\nu}\Psi\partial^{\nu}\Psi^{\dagger}-m_e^2\Psi\Psi^{\dagger}, \tag{5.15}$$

$$H^{\gamma}=\frac{1}{2}(\partial_{\nu}A)^2-\frac{m_{\gamma}^2}{2}A^2,$$

and the T-matrix interacting Hamiltonian $H_{\rm in}$ reads

$$H_{\rm in}=\frac{\lambda}{2}\Phi^2\phi\phi^{\dagger}+\left(eA+\frac{e^2}{2}A^2\right)\Psi\Psi^{\dagger}+\left(eA+\frac{e^2}{2}A^2\right)\phi\phi^{\dagger}.$$

It is usually argued [15,16] that the interacting pieces in H^{hb} can be dropped provided that $t_i\to-\infty$ and $t_f\to\infty$. Since we assume that ''pions'' are prepared in the remote past and ''muons'' are measured in the remote future, we shall accept in the following this omission. Among others, the former allows us to use safely Wick's theorem (2.16) and Dyson-Schwinger equation (2.18).

We can now approach calculating both the photon and electron number spectrum, i.e., $d\Delta\langle N_{\gamma}(\omega)\rangle/d\omega$ and $d\Delta\langle N_e(\omega)\rangle/d\omega$, respectively. As for $d\Delta\langle N_{\gamma}(\omega)\rangle/d\omega$, an order-$e^2$ contribution is clearly done only by diagrams in Fig. 7 as there are no relevant graphs with electron vertices contributing to this order, and so Eqs. (5.10) and (5.13) still remain true. On the other hand, there is no order-e^2 contribution to $d\Delta\langle N_e(\omega)\rangle/d\omega$. The lowest order in e (keeping λ^2 fixed) is e^4. This brings richer diagrammatic structure than in the photon case. In Fig. 10 we list all the generating thermal diagrams contributing to an order e^4.

It is easy to see that out of these 6 generating thermal diagrams we get 43 nonvanishing and topologically inequivalent modified cut diagrams; for example, from Fig. 10(c) we have only those diagrams which are depicted in Fig. 11. Note that the graphs of Fig. 11 must be multiplied by a factor of four as there are two equivalent insertions of the modified electron line and two equivalent distributions of the photon-muon vertex (so together with 1/2! from a Taylor expansion of the T matrix we get the symmetry factor 2). Analogously we get ten inequivalent modified cut diagrams from Fig. 10(a); seven from (b); eight from (d); six from (e), and eight from (f). The actual electron number spectrum calculations are thus rather involved.

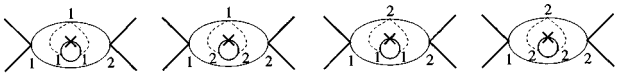

FIG. 11. The nonvanishing modified cut diagrams from Fig. 10(c).

Nevertheless, one might evaluate fairly quickly $F^{\rm emission}(\omega_e)+F^{\rm absorption}(\omega_e)$ as there are only three diagrams which contribute, namely,

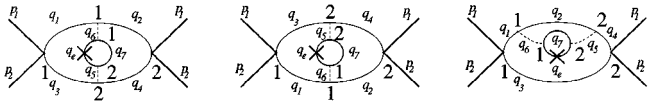

Let us recall that in the final state we must have, apart from the heat bath particles, only two ''muons,'' and so the diagram

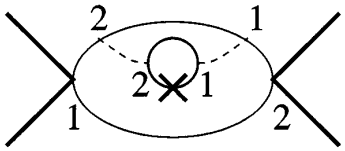

cannot contribute to $d\Delta\langle N_e(\omega)\rangle/d\omega$. Subtracting a temperature-independent part, we are left with

$$\begin{aligned}F^{\rm emission}(\omega_e)+F^{\rm absorption}(\omega_e)&\\ =\frac{t\lambda^2e^4f_B(\omega_e)}{\langle T\mathcal{P}T^{\dagger}\rangle_{p_1p_2,\beta}V\omega_{p_1}\omega_{p_2}(2\pi)^8}&\\ \times\int d^4q_7d^4q_e\delta^{+}(q_7^2-m_e^2)\delta(q_e^2-m_e^2)\delta(q_e^0-\omega_e)&\\ \times\int d^4q_2d^4q_3\delta^{+}(q_2^2-m_{\mu}^2)\delta^{+}(q_3^2-m_{\mu}^2)&\\ \times\{K_1\delta^4(-Q+q_2+q_3+q_7-q_e)&\\ -K_2\delta^4(-Q+q_2+q_3+q_7+q_e)\},&\end{aligned} \tag{5.16}$$

with

$$K_1=\frac{1}{(-q_2Q+Q^2+i\epsilon)}\frac{1}{(-q_3Q+Q^2-i\epsilon)}\times\frac{1}{(-2q_7q_e+2m_e^2-m_{\gamma}^2)^2},$$

$$K_2=K_1(q_e\to-q_e).$$

If we are interested in the qualitative behavior of Eq. (5.16) at small ω's, one needs to perform an integration over p_e only. In order to keep our calculations as simple as possible, let us assume that $m_e=m_{\gamma}=0$. Equation (5.16) can now be handled in a similar way as in the photon heat bath case. We first perform a transformation

$$q_7 \to q_7 \mp q_e ,$$

$$q_e \to q_e .$$

So Eq. (5.16) now reads

$$\text{Eq. (5.16)} = \frac{t\lambda^2 e^4 f_B(\omega_e)}{\langle T\mathcal{P}T^\dagger\rangle_{p_1p_2,\beta} V\omega_{p_1}\omega_{p_2}(2\pi)^8} \times \int d^4q_2 d^4q_3 \delta^+(q_2^2-m_\mu^2)\delta^+(q_3^2-m_\mu^2) \times \frac{1}{(-q_2Q+Q^2+i\epsilon)} \frac{1}{(-q_3Q+Q^2-i\epsilon)} B, \tag{5.17}$$

where

$$B = \int \frac{d^4q_7 d^4q_e}{(2q_7q_e)^2}\{\delta^+(q_7^2+X)-\delta^+(q_7^2-X)\}\delta(q_e^2) \times \delta(q_7^0-\omega_e)\delta^4(-Q+q_2+q_3+q_7),$$

with $X=2q_7q_e$. As before we might expand B in terms of X. The first surviving term reads

$$B \sim \int d^4q_7 d^4q_e[\partial_{q_7^2}\delta(q_7^2)]\delta^4 \times(-Q+q_2+q_3+q_7)\frac{2X}{(2q_7q_e)^2} = -\omega_e^0\partial_{m^2}\int d^4q_7\delta(q_7^2-m^2)\delta^4(-Q+q_2+q_3+q_7) \times \frac{1}{|\mathbf{q}_7|}\ln\left(\frac{q_7^0-|\mathbf{q}_7|}{q_7^0+|\mathbf{q}_7|}\right)\Bigg|_{m=0}, \tag{5.18}$$

and so $B\propto\omega_e^0$, and consequently $F^{\text{emission}}(\omega_e)+F^{\text{absorption}}(\omega_e)\propto\omega_e^{-1}$. Straightforward application of the previous mathematical operations to $F^{\text{fluct}}(\omega_e)$ reveals that $F^{\text{fluct}}(\omega_e)\propto\omega_e^{-1}$ as well. Let us mention that the separate contributions present in $F^{\text{emission}}(\omega_e)$, $F^{\text{absorption}}(\omega_e)$, and $F^{\text{fluct}}(\omega_e)$, behave as ω_e^{-2} but they mutually cancel, leaving behind terms proportional at worst to ω_e^{-1}.

Surprisingly enough, we have found that, for small ω, our heat bath (5.15) changes due to scattering $\Phi\Phi\to\phi\bar{\phi}$ in such a way that the rate of change in the electron number spectrum has qualitatively similar behavior (i.e., ω^{-1}) as the rate of change in the photon number spectrum. This is so provided one assumes that both electrons and photons are massless particles. Clearly, ω^{-2} behavior would be disastrous as it would suggest that the energy density $\omega\, dN/d\omega$ of the heat bath particles behaves as ω^{-1} which would, if integrated, produce an infinite contribution to the total energy carried off by the heat-bath particles.

VI. CONCLUSIONS

In this paper we have formulated a systematic method for studying the heat bath particle number spectrum using modified cut diagrams. In particular, for the quark-gluon plasma in thermodynamical equilibrium our approach should be useful as an effective alternative to the Landshoff-Taylor [3] approach. The method used in [3] (i.e., to start from first principles) suffers from the lack of a systematic computational approach for higher orders in coupling constants. One of the cornerstones of our formalism is the largest-time equation (LTE). We have shown how the zero-temperature LTE can be extended to finite temperature. During the course of this analysis, we have emphasized some important properties of the finite-temperature extension which are worth mentioning. First, many of the kinematic rules valid for zero-temperature diagrams cannot be directly used in the finite-temperature ones. This is because the emission or absorption of heat bath particles make it impossible to fix some particular direction to a diagrammatic line. It turns out that one finds more diagrams than one used to have at zero temperature. The most important reductions of the diagrams have been proved. The rather complicated structure of the finite-temperature diagrams brings into play another complication: uncuttable diagrams. It is well known that at zero temperature one can always make only one cut in each cut diagram (this can be viewed as a consequence of the unitarity condition). This is not true, however, at finite temperature. We have found it as useful to start fully with the LTE analysis which is in terms of type-1 and type-2 vertices. This language allows us to construct systematically all the cut diagrams. We have refrained from an explicit use of the cuts in finite-temperature diagrams as those are ambiguous and therefore rather obscure the analysis.

The second, rather technical, corner stone is the thermal Dyson-Schwinger equation. We have developed a formalism of the *arrowed* variations acting directly on field operators. This provides an elegant technique for dealing in a practical fashion with expectation values (both thermal and vacuum) whenever functions or functionals of fields admit the decomposition (A1). The merit of the Dyson-Schwinger equation is that it allows us to rewrite an expectation value of some functional of the field in terms of expectation values of less complicated functionals. Some illustrations of this and further thermal functional identities are derived in the Appendix.

When we have studied the heat bath particle number spectrum, we applied the Dyson-Schwinger equation both to the numerator and denominator of the corresponding expression. The results were almost the same. A simple modification of one propagator rendered both equal. We could reflect this on a diagrammatical level very easily as the denominator was fully expressible in terms of thermal cut diagrams. Our final rule for the heat bath particle spectrum is

$$\frac{d\Delta\langle N(\omega)\rangle}{d\omega} = \frac{\langle T^\dagger\mathcal{P}T\rangle^M_{p_1p_2,\beta}}{\langle T^\dagger\mathcal{P}T\rangle_{p_1p_2,\beta}}, \tag{6.1}$$

with T being the T matrix, $\mathcal{P}$ being the projection operator onto final states, p_1, p_2 being the momenta of particles in the initial state, β being the inverse temperature, and M being an abbreviation for the modified diagrams. Modification of the cut diagrams consists of the substitution in turn of each heat bath particle line by an altered one. This substitution must be done in each cut diagram. Replacement must be only one per

modified diagram. Our approach is demonstrated on a simple model where two scalar particles (''pions'') scatter, within a photon heat bath, into a pair of charged particles (''muon'' and ''antimuon'') and we explicitly calculate the resulting changes in the number spectra of the photons. It is also discussed how the results will change if the photon heat bath is replaced with a photon-electron one.

ACKNOWLEDGMENTS

We are indebted to P. V. Landshoff for reading the manuscript and for invaluable discussions. This work is supported in part by Fitzwilliam College.

APPENDIX: FUNCTIONAL FORMALISM AND GENERAL BACKGROUND

Equation (2.18) gives us an alternative definition of Wick's theorem in terms of the ''functional derivation'' $\delta/\delta\psi(x)$. We refer to Eq. (2.18) as the Dyson-Schwinger equation because the classical $T=0$ Dyson-Schwinger equations are implied by it. Let us first show that Eq. (2.18) is consistent with Wick's theorem (2.16) and (2.17). To be specific, let us consider an ensemble of noninteracting particles in thermodynamical equilibrium. In order to keep the work transparent, we shall suppress all the internal indices. There is no difficulty whatsoever in reintroducing the necessary details. Let us first realize that for any (well-behaved) functional the following Taylor's expansion holds [17]:

$$X[\psi]=\sum_n \int dx_1\cdots\int dx_n \alpha^n(x_1,\ldots,x_n)\psi(x_1)\cdots\psi(x_n). \tag{A1}$$

The same is true if ψ is an operator instead. In the latter case the $\alpha^n(\cdots)$ are not generally symmetric[8] in the x's. When Fermi fields are involved, we might, for the sake of compactness, include in the argument of ψ the space-time coordinate, the Dirac index, and a discrete index which distinguishes ψ_α from $\overline{\psi}_\alpha$. In the latter case $\int dx\to\Sigma\int dx$, where the summation runs over the discrete indices. With this convention, the expansion (A1) holds even for the Fermi fields. An extension of Eq. (A1) to the case where different fields are present is natural. Particularly important is the case when ψ is a field in the interaction picture; using Wick's theorem and decomposition (A1) one can then write

$$\begin{aligned}\langle G[\psi]\psi(x)F[\psi]\rangle_\beta &= \sum_{m,n}\left(\int dx\right)^n\left(\int dy\right)^m \alpha^n(x_1,\ldots,x_n)\beta^m(y_1,\ldots,y_m)\left\langle\left(\prod_k^n \psi(x_k)\right)\psi(x)\prod_{k'}^m \psi(y_{k'})\right\rangle_\beta \\ &= \sum_n\left(\int dx\right)^n \alpha^n(x_1,\ldots,x_n)\sum_l^n (\pm1)^{n-l}\langle\psi(x_l)\psi(x)\rangle_\beta\left\langle\prod_{k\neq l}^n \psi(x_k)F[\psi]\right\rangle_\beta \\ &\quad+\sum_m\left(\int dy\right)^m\beta^m(y_1,\ldots,y_m)\sum_l^m (\pm1)^{l-1}\langle\psi(x)\psi(x_l)\rangle_\beta\left\langle G[\psi]\prod_{k'\neq l}^m \psi(y_{k'})\right\rangle_\beta,\end{aligned} \tag{A2}$$

with $(\int dx)^n=\int dx_1\cdots\int dx_n$. The ''$-$'' stands for fermions and ''$+$'' for bosons. On the other hand, using the formal prescriptions (2.19) and (2.21) for $\vec{\delta}/\delta\psi(x)$ one can read

$$\begin{aligned}&\int dz\langle\psi(x)\psi(z)\rangle_\beta\left\langle G[\psi]\frac{\vec{\delta}F[\psi]}{\delta\psi(z)}\right\rangle_\beta \\ &\quad=\sum_m\left(\int dy\right)^m\beta^m(y_1,\ldots,y_m)\int dz\langle\psi(x)\psi(z)\rangle_\beta\sum_l^m (\pm1)^{l-1}\delta(z-y_l)\left\langle G[\psi]\prod_{k'\neq l}^m \psi(y_{k'})\right\rangle_\beta \\ &\quad=\sum_m\left(\int dy\right)^m\beta^m(y_1,\ldots,y_m)\sum_l^m (\pm1)^{l-1}\langle\psi(x)\psi(y_l)\rangle_\beta\left\langle G[\psi]\prod_{k'\neq l}^m \psi(y_{k'})\right\rangle_\beta.\end{aligned} \tag{A3}$$

A similar expression holds for $\int dz\langle\psi(x)\psi(z)\rangle_\beta\langle\{G[\psi]\vec{\delta}/\delta\psi(z)\}F[\psi]\rangle_\beta$. Putting the latter two together we get precisely Eq. (A2). This confirms the validity of Eq. (2.18). It is easy to persuade oneself that exactly the same sort of arguments leads to

$$\langle\psi(x)F[\psi]\rangle_\beta=\int dz\langle\psi(x)\psi(z)\rangle_\beta\left\langle\frac{\vec{\delta}F[\psi]}{\delta\psi(z)}\right\rangle_\beta, \tag{A4}$$

[8]If $X=X[\psi,\partial\psi]$, the α^n may also contain derivations working on the various fields.

$$\langle \mathcal{T}\{\psi(x)F[\psi]\}\rangle_\beta = \int dz \langle \mathcal{T}[\psi(x)\psi(z)]\rangle_\beta \left\langle \mathcal{T}\left(\frac{\vec{\delta}F[\psi]}{\delta\psi(z)}\right)\right\rangle_\beta , \tag{A5}$$

$$\langle G[\psi]\mathcal{T}\{\psi(x)F[\psi]\}\rangle_\beta = \int dz \langle \mathcal{T}[\psi(x)\psi(z)]\rangle_\beta \left\langle G[\psi]\mathcal{T}\left(\frac{\vec{\delta}F[\psi]}{\delta\psi(z)}\right)\right\rangle_\beta + \int dz \langle \psi(z)\psi(x)\rangle_\beta \left\langle \frac{G[\psi]\overleftarrow{\delta}}{\delta\psi(z)}\,\mathcal{T}(F[\psi])\right\rangle_\beta , \tag{A6}$$

etc., with $\mathcal{T}$ being either the chronological or antichronological time ordering symbol. At this stage it is important to realize that from the definition of $\vec{\delta}/\delta\psi(x)$ directly follows that $[\vec{\delta}/\delta\psi(x);\vec{\delta}/\delta\psi(y)]_\mp = 0$ (''$-$'' holds for bosons and ''$+$'' for fermions). Indeed,

$$\frac{\vec{\delta}^2F[\psi]}{\delta\psi(x)\,\delta\psi(y)} = \sum_{n=2}\sum_{i<j}\left(\int dx\right)^{n-2}[\alpha^n(x_1\ldots\overset{x_i}{\downarrow}x\ldots\overset{x_j}{\downarrow}y\ldots x_n)\pm\alpha^n(x_1\ldots\overset{x_i}{\downarrow}y\ldots\overset{x_j}{\downarrow}x\ldots x_n)](\pm1)^{i+j}\prod_{m\neq i,j}^{n}\psi(x_m) = \mp\frac{\vec{\delta}^2F[\psi]}{\delta\psi(y)\,\delta\psi(x)}. \tag{A7}$$

Similarly $[\vec{\delta}/\delta\psi(x);\vec{\delta}/\delta\psi(y)]_\mp = 0$. Analogously we might prove

$$\frac{F[\psi]\overleftarrow{\delta}^2}{\delta\psi(x)\,\delta\psi(y)k} = \frac{\vec{\delta}^2F[\psi]}{\delta\psi(x)\,\delta\psi(y)} \tag{A8}$$

and

$$\frac{\vec{\delta}^2(F[\psi]G[\psi])}{\delta\psi(x)\,\delta\psi(y)} = \frac{F[\psi]\overleftarrow{\delta}^2}{\delta\psi(x)\,\delta\psi(y)}G[\psi] + (-1)^p\frac{F[\psi]\overleftarrow{\delta}}{\delta\psi(x)}\frac{\vec{\delta}G[\psi]}{\delta\psi(y)} + \frac{F[\psi]\overleftarrow{\delta}}{\delta\psi(y)}\frac{\vec{\delta}G[\psi]}{\delta\psi(x)} + F[\psi]\,\frac{\vec{\delta}^2G[\psi]}{\delta\psi(x)\,\delta\psi(y)}. \tag{A9}$$

The p is 0 for bosons and 1 for fermions. With Eqs. (2.18) and (A4)–(A6) one can easily construct more complicated expectation values. For example, using Eqs. (2.18) and (A4) we get

$$\begin{aligned}\langle\psi(x)\psi(y)F[\psi]\rangle_\beta = \int \frac{dz_1dz_2}{2}[\langle\psi(x)\psi(z_1)\rangle_\beta\langle\psi(y)\psi(z_2)\rangle_\beta + (-1)^p\langle\psi(x)\psi(z_2)\rangle_\beta\langle\psi(y)\psi(z_1)\rangle_\beta]\left\langle\frac{\vec{\delta}^2F[\psi]}{\delta\psi(z_1)\,\delta\psi(z_2)}\right\rangle_\beta \\ + \langle\psi(x)\psi(y)\rangle_\beta\langle F[\psi]\rangle_\beta .\end{aligned} \tag{A10}$$

Similarly, using Eq. (2.18) and (anti)commutativity of the arrowed $\delta/\delta\psi(x)$, we get

$$\begin{aligned}\langle G[\psi]\psi(x)\psi(y)F[\psi]\rangle_\beta = \int \frac{dz_1dz_2}{2}[\langle\psi(x)\psi(z_1)\rangle_\beta\langle\psi(y)\psi(z_2)\rangle_\beta + (-1)^p\langle\psi(x)\psi(z_2)\rangle_\beta\langle\psi(y)\psi(z_1)\rangle_\beta] \\ \times\left\langle G[\psi]\frac{\vec{\delta}^2F[\psi]}{\delta\psi(z_1)\,\delta\psi(z_2)}\right\rangle_\beta + \int \frac{dz_1dz_2}{2}[\langle\psi(z_1)\psi(x)\rangle_\beta\langle\psi(z_2)\psi(y)\rangle_\beta \\ + (-1)^p\langle\psi(z_2)\psi(x)\rangle_\beta\langle\psi(z_1)\psi(y)\rangle_\beta]\left\langle\frac{G[\psi]\overleftarrow{\delta}^2}{\delta\psi(z_1)\,\delta\psi(z_2)}F[\psi]\right\rangle_\beta \\ + \int dz_1dz_2[\langle\psi(z_1)\psi(x)\rangle_\beta\langle\psi(y)\psi(z_2)\rangle_\beta \\ + (-1)^p\langle\psi(x)\psi(z_2)\rangle_\beta\langle\psi(z_1)\psi(y)\rangle_\beta] \\ \times\left\langle\frac{G[\psi]\overleftarrow{\delta}}{\delta\psi(z_1)}\frac{\vec{\delta}F[\psi]}{\delta\psi(z_2)}\right\rangle_\beta + \langle\psi(x)\psi(y)\rangle_\beta\langle G[\psi]F[\psi]\rangle_\beta .\end{aligned} \tag{A11}$$

We could proceed further having still higher powers of fields and variations. However, there is a quite interesting generalization in the case when we have (anti-)time-ordered operators. Let us have $F[\psi]=\mathcal{T}(F[\psi])$; in this case,

$$\langle F[\psi]\rangle_\beta=\sum_n \left(\int dx\right)^n \alpha^n(\cdots)\left\langle \mathcal{T}\left(\prod_{i=1}^n \psi(x_i)\right)\right\rangle_\beta = \sum_{n=1}\left(\int dx\right)^n \frac{\alpha^n(\cdots)}{n}\sum_{i,j}\varepsilon_P\langle \mathcal{T}[\psi(x_i)\psi(x_j)]\rangle_\beta$$
$$\times\left\langle \mathcal{T}\left(\prod_{m\neq i,j}\psi(x_m)\right)\right\rangle_\beta + \alpha^0(\cdots)$$
$$= \int dz_1 dz_2 \langle \mathcal{T}[\psi(z_1)\psi(z_2)]\rangle_\beta \left\langle \frac{\vec{\delta}^2\overline{F}[\psi]}{\delta\psi(z_2)\delta\psi(z_1)}\right\rangle_\beta + \langle F[0]\rangle_\beta, \tag{A12}$$

where $\overline{F}[\psi]$ differs from $F[\psi]$ in the replacement $\alpha^n(\cdots)\to\alpha^n(\cdots)/n$ (n starts from 1). In comparison with Eqs. (A4)–(A11), the $\alpha^0(\cdots)$ (i.e., the pure $T=0$ contribution) does matter here. Note that $\alpha^0(\cdots)$ generally involves non-heat-bath fields with corresponding space-time integrations. A similar extension is true if $F[\psi]=\mathcal{T}_C(F[\psi])$, where $\mathcal{T}_C$ is the time path ordering symbol. In that case

$$\langle F[\psi]\rangle_\beta=\sum_n\left(\int_C dx\right)^n\alpha^n(\ldots)\left\langle \mathcal{T}_C\left(\prod_{p=1}^n\psi(x_p)\right)\right\rangle_\beta$$
$$= \int_C dz_1 dz_2\langle \mathcal{T}_c[\psi(z_1)\psi(z_2)]\rangle_\beta\left\langle\frac{\vec{\delta}^2\overline{F}[\psi]}{\delta\psi(z_2)\delta\psi(z_1)}\right\rangle_\beta + \langle F[0]\rangle_\beta, \tag{A13}$$

with[9] $\int_C dx=\int_C dt\int_V d\mathbf{x}$ and $\delta\psi(x)/\delta\psi(y)=\delta_C(x-y)$. Wick's theorem for the $\mathcal{T}_C$-oriented product of fields has an obvious form

$$\langle \mathcal{T}_C[\psi(x_1)\cdots\psi(x_{2n})]\rangle_\beta=\sum_{\substack{j\\ j\neq i}}\varepsilon_P\langle\mathcal{T}_C[\psi(x_i)\psi(x_j)]\rangle_\beta \times\left\langle\mathcal{T}_C\left(\prod_{k\neq i;j}\psi(x_k)\right)\right\rangle_\beta. \tag{A14}$$

This can be directly derived from Wick's theorem (2.17), realizing that

$$\mathcal{T}_C[\psi(x_1)\cdots\psi(x_m)]=\sum_P \varepsilon_P\theta_C(t_{P_1},\ldots,t_{P_m})\psi(x_{P_1})\ldots \times\psi(x_{P_m}), \tag{A15}$$

where P refers to the permutation of the indices and $\theta_C(t_1,\ldots,t_m)$ being a contour step function [19] defined as

$$\theta_C(t_1,\ldots,t_m)=\begin{cases}1 & (t_1,\ldots,t_m \text{ are } \mathcal{T}_C \text{ oriented along } C),\\ 0 & (\text{otherwise}).\end{cases} \tag{A16}$$

[9]A contour δ function $\delta_C(x-y)$ is defined as $\int_C dz\,\delta_C(z-z')f(z)=f(z')$; see [9,18].

Particularly important is the Keldysh-Schwinger path [1,19,20]; see Fig. 12.

In the latter case

$$\langle F[\psi]\rangle_\beta=\int_{C_1}dz_1dz_2\langle\mathcal{T}[\psi(z_1)\psi(z_2)]\rangle_\beta \times\left\langle\frac{\vec{\delta}^2\overline{F}[\psi]}{\delta\psi(z_2)\delta\psi(z_1)}\right\rangle_\beta + \int_{C_2}dz_1dz_2\langle\overline{\mathcal{T}}[\psi(z_1)\psi(z_2)]\rangle_\beta \times\left\langle\frac{\vec{\delta}^2\overline{F}[\psi]}{\delta\psi(z_2)\delta\psi(z_1)}\right\rangle_\beta + 2\int_{C_2}dz_1\int_{C_1}dz_2\langle\psi(z_1) \times\psi(z_2)\rangle_\beta\left\langle\frac{\vec{\delta}^2\overline{F}[\psi]}{\delta\psi(z_2)\delta\psi(z_1)}\right\rangle_\beta + \langle F[0]\rangle_\beta. \tag{A17}$$

Application to the product $G[\psi]F[\psi]$ with $F[\psi]=\mathcal{T}_{C_1}(F[\psi])$ and $G[\psi]=\mathcal{T}_{C_2}(G[\psi])$ is straightforward and reads

$$\langle G[\psi]F[\psi]\rangle_\beta=\int dz_1dz_2\langle\overline{\mathcal{T}}[\psi(z_1)\psi(z_2)]\rangle_\beta \times\left\langle\overline{\frac{G[\psi]\vec{\delta}^2}{\delta\psi(z_2)\delta\psi(z_1)}F[\psi]}\right\rangle_\beta + \int dz_1dz_2\langle\mathcal{T}[\psi(z_1)\psi(z_2)]\rangle_\beta \times\left\langle\overline{G[\psi]\frac{\vec{\delta}^2F[\psi]}{\delta\psi(z_2)\delta\psi(z_1)}}\right\rangle_\beta + 2\int dz_1dz_2\langle\psi(z_1)\psi(z_2)\rangle_\beta \times\left\langle\overline{\frac{G[\psi]\vec{\delta}}{\delta\psi(z_1)}\frac{\vec{\delta}F[\psi]}{\delta\psi(z_2)}}\right\rangle_\beta + \langle G[0]F[0]\rangle_\beta, \tag{A18}$$

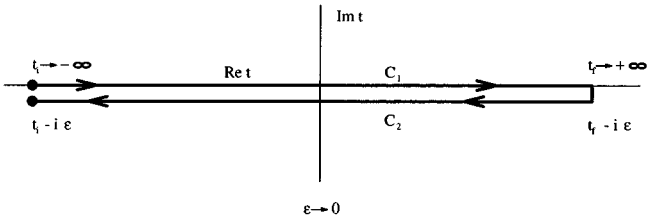

FIG. 12. The Keldysh-Schwinger time path.

where the overbar indicates that we work with $\alpha^n(\cdots)\beta^m(\cdots)/(n+m)$ instead of $\alpha^n(\cdots)\beta^m(\cdots)$; we have also abbreviated $\int_{C_1} dz$ to $\int dz \int_{C_1} dz$. We should also emphasize that $\delta\psi(x)/\delta\psi(y)$ used in Eq. (A18) is $\delta(x-y)$ rather than $\delta_C(x-y)$.

In Eq. (4.3) the inverted version of Eq. (A18) has been used, namely,

$$\langle (G[\psi]F[\psi])' \rangle_\beta = \int \frac{dz_1 dz_2}{2} \langle \overline{\mathcal{T}}[\psi(z_1)\psi(z_2)] \rangle_\beta \times \left\langle \frac{G[\psi]\vec{\delta}^2}{\delta\psi(z_2)\,\delta\psi(z_1)} F[\psi] \right\rangle_\beta + \int \frac{dz_1 dz_2}{2} \langle \mathcal{T}[\psi(z_1)\psi(z_2)] \rangle_\beta \times \left\langle G[\psi] \frac{\vec{\delta}^2 F[\psi]}{\delta\psi(z_2)\,\delta\psi(z_1)} \right\rangle_\beta + \int dz_1 dz_2 \langle \psi(z_1)\psi(z_2) \rangle_\beta \times \left\langle \frac{G[\psi]\vec{\delta}}{\delta\psi(z_1)} \frac{\vec{\delta} F[\psi]}{\delta\psi(z_2)} \right\rangle_\beta . \tag{A19}$$

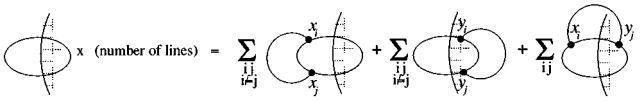

FIG. 13. Diagrammatic equivalent of Eq. (A19). The cut separates areas constructed out of $F[\psi]$ and $G[\psi]$.

Here $(G[\psi]F[\psi])'$ has the coefficients $\alpha^n(\cdots)\beta^m(\cdots)(n+m)/2$ instead of $\alpha^n(\cdots)\beta^m(\cdots)$. Note, that the $\alpha^0(\cdots)\beta^0(\cdots)$ does not contribute and thus we do not have any pure $T=0$ contributions. Equation (A19) has a natural interpretation. While the LHS tells us that from each thermal diagram [constructed out of $\langle G[\psi]F[\psi] \rangle_\beta$ with $(n+m)/2$ internal heat bath particle lines] we must take $n+m$ identical copies, the RHS says that this is virtually because we sum over all possible distributions of one heat bath particle line inside of the given diagram. The pictorial expression of Eq. (A19) is depicted in Fig. 13.

[1] M. LeBellac, *Thermal Field Theory* (Cambridge University Press, Cambridge, England, 1996).
[2] N. P. Landsman and Ch. G. van Weert, Phys. Rep. **145**, 141 (1987).
[3] P. V. Landshoff and J. C. Taylor, Nucl. Phys. **B430**, 683 (1994).
[4] P. V. Landshoff, Phys. Lett. B **386**, 291 (1966).
[5] L. V. Keldysh, Sov. Phys. JETP **20**, 1018 (1964).
[6] P. van Nieuwenhuizen, *Canonical Methods in Quantized Gauge Field Theories*, Teyler's lectures, Leyden University, 1992 (Leyden University, Leyden, The Netherlands, 1992).
[7] M. Veltman, *Diagrammatica—The Path to Feynman Diagrams* (Cambridge University Press, Cambridge, England, 1994).
[8] G. 't Hooft and M. Veltman, Diagrammar, CERN Yellow Report No. 73-9, 1993.
[9] R. Mills, *Propagators for Many-Particle Systems* (Gordon and Breach, New York, 1969).
[10] T. S. Evans and D. A. Steer, Nucl. Phys. **B474**, 481 (1996).
[11] C. Itzykson and J. B. Zuber, *Quantum Field Theory* (McGraw-Hill, New York, 1980).
[12] R. L. Kobes and G. W. Semenoff, Nucl. Phys. **B272**, 329 (1986).
[13] P. V. Landshoff and A. Rebhan, Nucl. Phys. **B410**, 23 (1993).
[14] M. Jacob and P. V. Landshoff, Phys. Lett. B **281**, 114 (1992).
[15] A. J. Niemi and G. W. Semenoff, Nucl. Phys. **B230**, 181 (1984).
[16] T. S. Evans and A. C. Pearson, Phys. Rev. D **52**, 4652 (1995).
[17] P. Ramond, *Field Theory, A Modern Primer* (Benjamin/Cummings, London, 1981).
[18] A. J. Niemi and G. W. Semenoff, Ann. Phys. (N.Y.) **152**, 105 (1984).
[19] M. van Eijck, Ph.D. thesis, University of Amsterdam, 1995.
[20] J. I. Kapusta and P. V. Landshoff, J. Phys. G **15**, 267 (1989).